# Geotechnical Study of Raspadalica Cliff Rockfall, Croatia

**Udovič, Dalibor; Kordić, Branko; Arbanas, Željko**

*Source / Izvornik:* **Applied Sciences, 2022, 12**

**Journal article, Published version**
**Rad u časopisu, Objavljena verzija rada (izdavačev PDF)**

https://doi.org/10.3390/app12136532

*Permanent link / Trajna poveznica:* https://urn.nsk.hr/urn:nbn:hr:157:570794

*Rights / Prava:* Attribution 4.0 International/Imenovanje 4.0 međunarodna

*Download date / Datum preuzimanja:* **2024-05-20**

Image not found or type unknown

*Repository / Repozitorij:*

Repository of the University of Rijeka, Faculty of Civil Engineering - FCERI Repository

UNIRI DIGITALNA KNJIŽNICA

Image not found or type unknown

applied sciences

IMPACT FACTOR 2.7

CITESCORE 4.5

Article

# Geotechnical Study of Raspadalica Cliff Rockfall, Croatia

Dalibor Udovič, Branko Kordić and Željko Arbanas

Special Issue
Structural Mechanics of Rocks and Rock Masses
Edited by
Dr. Pietro Mosca, Dr. Sabrina Bonetto and Dr. Chiara Caselle

MDPI

https://doi.org/10.3390/app12136532

applied sciences

MDPI

*Article*

# Geotechnical Study of Raspadalica Cliff Rockfall, Croatia

**Dalibor Udovič [1], Branko Kordić [2] and Željko Arbanas [3,*]**

[1] Monterra Ltd., Vukovarska 76, 51000 Rijeka, Croatia; dalibor.udovic@monterra.hr
[2] Croatian Geological Survey, Sachsova 2, 10000 Zagreb, Croatia; branko.kordic@hgi-cgs.hr
[3] Faculty Civil Engineering, University of Rijeka, Radmile Matejčić 3, 51000 Rijeka, Croatia
* Correspondence: zeljko.arbanas@gradri.uniri.hr; Tel.: +385-51-265-936

**Abstract:** The Raspadalica Cliff is an almost vertical 100 m high limestone cliff with a railway line at its foot and is known for numerous rockfall occurrences in the past. This article presents the results of the geotechnical study of the cliff based on a traditional geological and geotechnical field survey and remote sensing analysis. Both the traditional geological and geotechnical field survey and remote sensing surveys and analyses enabled the establishment of the structural model of the Raspadalica Cliff and the determination of the discontinuity sets and discontinuity features, such as orientation, spacing, persistence, roughness, discontinuity wall strength, aperture, degree of weathering of discontinuity wall, seepage conditions, and the presence and hardness of discontinuity filling. Kinematic analyses were performed on five cliff zones with slightly different structural features, indicating a relatively low probability of typical failures in the cliff rock mass that precede the rockfall occurrences. Although rockfall phenomena from the cliff face are relatively frequent, the kinematic analyses did not indicate a high probability of their occurrence. The aim of this manuscript is to make scientists and practitioners aware that investigation of rock mass cliffs and possible rockfall failures must not be based on usual methods without critical review of the obtained results and consequences. The combined use of traditional geological and geotechnical methods and more commonly used advanced remote sensing methods leads to better modelling, while the analysis of more associated failure modes can explain the triggering of rockfall.

**Keywords:** rockfall; cliff; unmanned aerial vehicle (UAV); photogrammetry; structure from motion (SfM); kinematic analysis

check for updates

**Citation:** Udovič, D.; Kordić, B.; Arbanas, Ž. Geotechnical Study of Raspadalica Cliff Rockfall, Croatia. *Appl. Sci.* **2022**, *12*, 6532. https://doi.org/10.3390/app12136532

Academic Editors: Sabrina Bonetto, Pietro Mosca and Chiara Caselle

Received: 29 August 2021
Accepted: 21 June 2022
Published: 28 June 2022

**Publisher's Note:** MDPI stays neutral with regard to jurisdictional claims in published maps and institutional affiliations.

**Copyright:** © 2022 by the authors. Licensee MDPI, Basel, Switzerland. This article is an open access article distributed under the terms and conditions of the Creative Commons Attribution (CC BY) license (https://creativecommons.org/licenses/by/4.0/).

## 1. Introduction

Rockfalls, by definition, are phenomena that include the detachment, falling, rolling, and bouncing of rock fragments from a slope, singly or in clusters, and the fragments may be defragmented during impact [1]. Occurrences can range from small fragments to massive blocks of different volumes and shapes falling, rolling, and bouncing down a slope [2,3]. Rockfall is one of the most frequent and dangerous types of landslides, which can cause numerous fatalities and high economic and social damage [4]. The high speed, mobility, and energy of falling rocks prevent fast responses by evacuation or protection [2,3,5,6].

The Raspadalica Cliff is an almost vertical 100 m high limestone slope (Figure 1) located at the contact of two geomorphological units, namely, the hilly Paleogene Flysch Basin and the elevated Ćićarija Mountain Range in the northern part of Istrian Peninsula, Croatia [7–9]. The wider Raspadalica location is known for numerous instabilities occurring as rockfalls from the Raspadalica Cliff, as well as landslides [10], that have previously caused significant damage to the railway line located on the slope made of flysch succession at the foot of the cliff.

In this paper we focus on rockfall occurrences from the Raspadalica Cliff, while the slides on the flysch slopes below the cliff, which also caused damage to railway facilities, are not mentioned in this manuscript. Although sliding of the flysch slopes have caused multiple interruptions of railway traffic as well as multiple slope stabilization measures,

the rockfall occurrences in the past were many times more dangerous and demanding for remediation.

**Figure 1.** A view of the Raspadalica Cliff, Istria Peninsula, Croatia. The rockfalls threatening the railway line on the slope are clearly visible.

The documented history of rockfalls from the Raspadalica Cliff dates back to 1951, when the railway technical office was faced with multiple traffic interruptions on the railway caused by several landslides and rockfalls that threatened the stability of the railway embankment and traffic safety. From 1951 to the present, numerous instabilities events have occurred followed by a series of field investigations, remediation designs and implementation of remedial measures, but the threat from rockfalls still exists.

In recent years traditional (conventional) geological and geotechnical methods as well as more commonly used advanced remote sensing methods have been used to describe geotechnical rock cliff models and to derive the geotechnical elements used in stability analysis and potential failures of rock mass defined by the positions and orientations of the rock joint systems. The Raspadalica Cliff is an example of a cliff characterized by its geotechnical features that renders use of only traditional geological and geotechnical methods (unavailability of individual parts of the cliff) or remote sensing methods (lower exposure of individual joint sets) impossible and affects the necessary combination of both methods. Additionally, kinematic analyses did not indicate a high probability of rockfall occurrence, although rockfall phenomena from the cliff face were relatively frequent in the past. The aim of this manuscript is to make scientists and practitioners aware that the investigation of rock mass cliffs and possible rockfall failures must not be based on usual methods without critical review of the obtained results and consequences. The combined use of traditional geological and geotechnical methods and more used advanced remote sensing methods leads to better modelling, while the analysis of more associated failure modes can explain the triggering of rockfall.

In order to determine the detailed geological structure of the cliff and the causes of rockfall occurrences at the Raspadalica Cliff, several campaigns of field investigations have been carried out over the last decade. The first, conducted for remedial measures and rockfall protection design, used the traditional methods of engineering geological surveying and mapping [11] and was limited to the rock mass at the foot of the cliff due to its height [12]. The second began in 2019 and was based on remote sensing techniques combined with data collected by traditional surveying. In the last decade remote sensing

techniques have been introduced to rock mass characterization with the aim of overcoming the disadvantages of traditional surveys, through the acquisition of 3D high resolution point clouds (3D HRPC) by non-contact measurements based on photogrammetry, airborne light detection and ranging (LiDAR), terrestrial laser scanning (TLS), and unmanned aerial vehicles (UAV) [13], where the remote sensing techniques applied were based on unmanned aerial vehicle (UAV) photogrammetry data.

In this research, the geotechnical model of the Raspadalica Cliff was established, based on HR 3DPC with about 32 million points generated from two UAV missions using both traditional geological and geotechnical field surveys and remote sensing analysis based on the recent achievements in remote sensing methods. The results of the combined methods allowed the extraction of the orientation space of the visible discontinuity planes as well as other discontinuity properties at five separate zones of the cliff, which differ slightly in terms of dip, discontinuity orientation, and other discontinuity properties. Based on the established geotechnical model of the cliff, statistical kinematic analyses were performed that indicated a relatively low probability of rockfall occurrence. The analysis of various instabilities determined that only a combination of two mechanisms could cause rock block detachment, likely in combination with additional processes, such as lateral stress relaxation; weathering and softening of joints in filling, freezing, and thawing processes; hydrostatic pressure from water in subvertical discontinuities; and temperature effects.

## 2. Site Description

### *2.1. Geographic and Geological Settings*

The Raspadalica Cliff is located in the northern part of the Istrian Peninsula in the northwestern part of the Croatian Adriatic coast at the boundary between the Paleogene Flysch Basin (i.e., Gray Istria) and the geomorphologically dominant elevation of the Ćićarija Mountain Range (i.e., White Istria). The Ćićarija Mountain Range mainly consists of carbonate rocks: Paleogene limestone (Figures 2 and 3). This area of the boundary of the Paleogene Flysch Basin and the Ćićarija Mountain Range is a part of the overthrust structure that stretches in a NW–SE direction. The kinematics of the rock units with different geotechnical behavior (rigid and ductile rock masses) at the boundary between the overthrust carbonate unit, the Ćićarija Mountain Range, and the Paleogene Flysch Basin, is based on the relationship between the relatively rigid (carbonate rocks) and relatively ductile (flysch rock complex) media during simultaneous deformations. The effects of deformation are most distinctive at the contact (overthrust zone) between the limestone and flysch rock complex. For this reason, the more ductile flysch rock mass is deformed by the relatively rigid limestone rock blocks. Recent gravitational slides of huge carbonate rock blocks over the flysch bedrock are also visible [7]. The flysch bedrock complex formed by turbidite sedimentations is lithologically very heterogeneous due to the frequent vertical and lateral alternations of different lithological sequences: marls, siltstones, fine-grained sandstones, and very distinct layers of calcarenites. In contrast to the karstified limestone rocks of the cliffs and the hill, the flysch bedrock is covered by Quaternary deposits. At the foot of the cliffs, the coarse-grained fragments originating from the cliffs have mixed with the silty clay from the flysch weathering zones, forming slope deposits of a few meters in length at the foot of the carbonate rock complex of the Ćićarija Mountain [7].

The Raspadalica Cliff is a part of the Ćićarija Mountain Range, built of Paleogene limestone, and the contact between the limestone rock mass of the cliff and the flysch rock complex in the lower part of the slope is a reverse fault dipping ~23 degrees towards the NE (Figures 3 and 4). The limestone mass is homogeneous, fine-grained, and well stratified. The thickness of beds ranges from 10 cm to 2 m with several interlayers of coal of several centimeters in thickness. The general dip of the bedding planes is relatively favorable for stability of the cliff and inclined toward the slope, with minor variations along the cliff. A detailed description of the geotechnical model of the cliff is described in the following sections.


**Figure 2.** Geographic location of the Raspadalica Cliff.

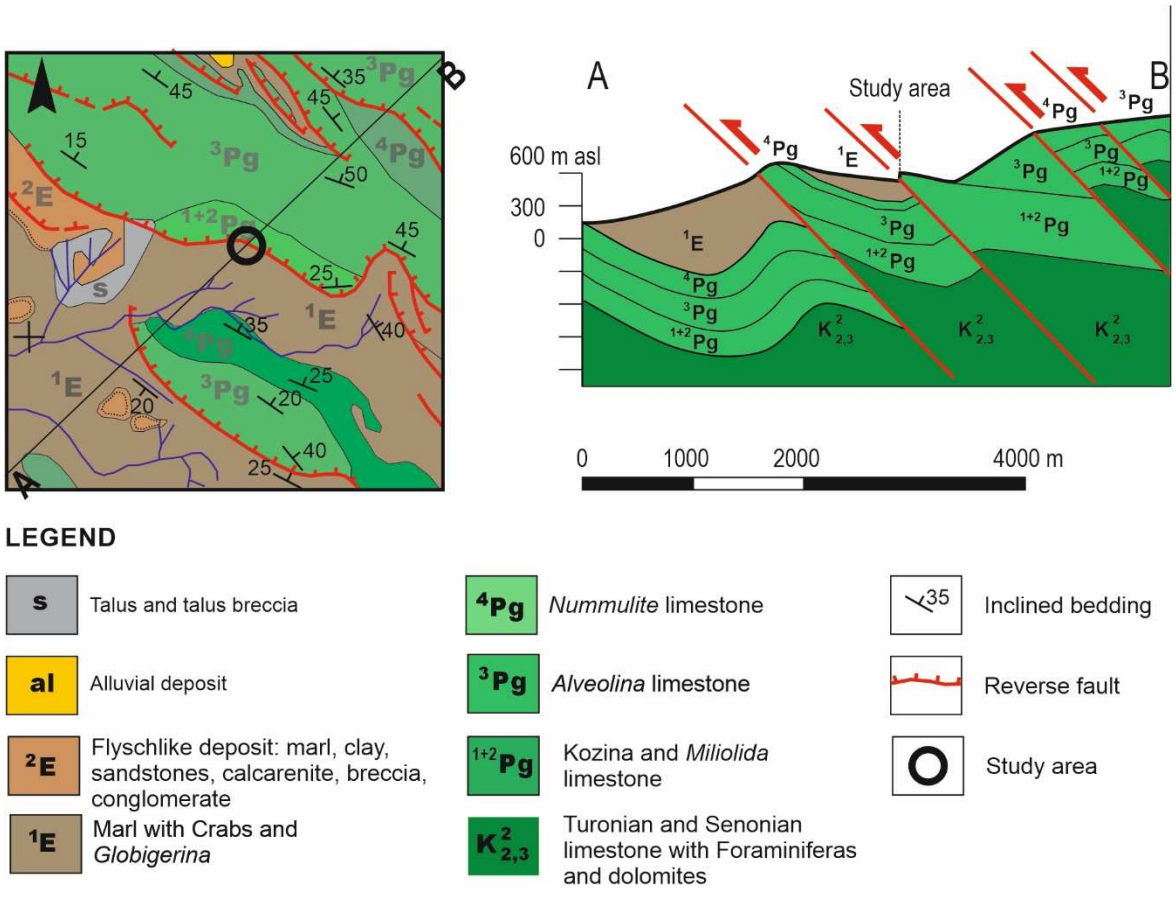


**Figure 3.** Geological map of the wider area of the Raspadalica Cliff: Geological map (**left**) and geological cross-section (**right**). Black circle indicates the Raspadalica Cliff location [8,9].

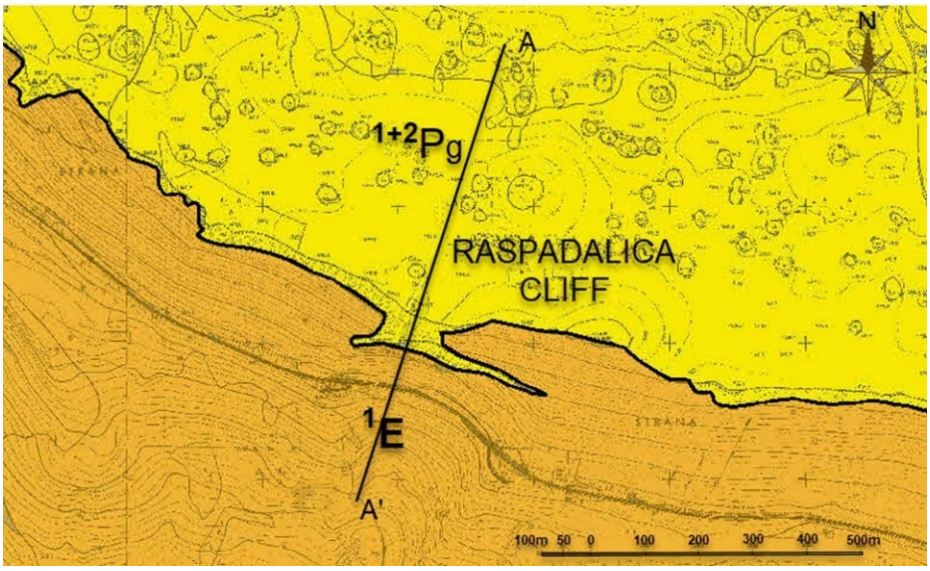


(**a**)

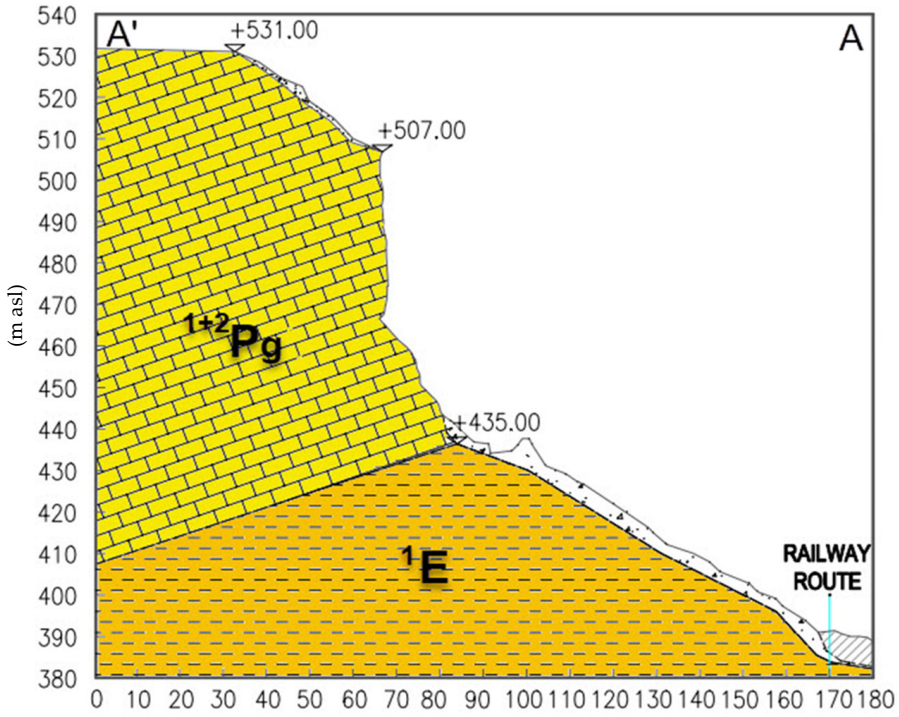


(**b**)

**Figure 4.** Geological map of the Raspadalica Cliff (**a**) and marked schematic cross-section (A–A'): (**b**). Overthrust limestone Lower and Middle Paleogene rock mass ($^{1+2}$Pg) lies on Lower Eocene flysch deposits ($^{1}$E). The flysch deposits are covered with talus material originating from a limestone cliff [12].

### *2.2. Raspadalica Cliff Rockfall History*

The railway line threatened by rockfalls from the Raspadalica Cliff is the part of the railway line that runs from the border between the Republic of Croatia and Slovenia to the City of Pula, the largest city on the Istria Peninsula, which connects Istria with the railway lines of the Fifth Pan European Corridor. The location of Raspadalica, where the railway line is located on the flysch deposits in the toe of the 100 m high carbonate rock cliff, is known for numerous slides that have caused considerable damage to the railway embankment

and rockfalls, which, in addition to breaking railway facilities, have threatened the lives of people and train traffic. The three most significant rockfalls occurred on 18 November 1975, causing fatalities, and on 11 August 1992 and 10 February 1999, causing significant damage to the railway facilities. The significant rockfalls recorded by the Railways Technical Office are listed in Table 1. There are no direct observations that accompanied registered rockfalls from the Raspadalica Cliff but, analyzing the circumstances in which the rockfalls were triggered, it is not possible to exclude any of listed influences on weakening of particular blocks in the cliff. Analyzing the weather conditions during the registered rockfall occurrences (listed in Table 1) it is possible to conclude that the decisive impact was caused by rainfall infiltration in vertical joints, causing a rise of hydrostatic pressure at the rock blocks in the cliff as well as an additional horizontal force necessary for rockfall triggering. Most of the registered rockfalls have occurred during rainfall events or during storms accompanied by high rainfall intensities. It is also remarkable that the dropped rock blocks were positioned in the middle part of the cliff face that were exposed to higher hydrostatic pressures than the blocks in the upper parts of the cliff.

**Table 1.** The rockfalls registered at the Raspadalica Cliff location by the Croatian Railways Technical Office.

| Date | Time | Rockfall Volume | Consequences | Note |
|---|---|---|---|---|
| 11 February 1963 | 21:48 | Unknown | Traffic interruption | - |
| 6 September 1964 | 16:52 | Unknown | Traffic interruption | - |
| 18 November 1975 | - | >500 $m^3$ | Facilities damage, human casualties | The train ran into rock blocks and slipped off the tracks |
| 16 March 1976 | 20:30 | Unknown | Traffic interruption | - |
| 28 May 1976 | 20:30 | Unknown | Traffic interruption | - |
| 28 January 1977 | 00:25 | Unknown | Traffic interruption | - |
| 2 March 1977 | 10:20 | Unknown | Traffic interruption | - |
| 7 May 1987 | 17:30 | Unknown | Traffic interruption | Damage to train bumper |
| 11 November 1987 | 01:45 | Unknown | Traffic interruption | The train stopped before the rock blocks |
| 21 December 1990 | 03:45 | ≈20 $m^3$ | Traffic interruption | - |
| 11 August 1992 | 14:15 | >500 $m^3$ | Traffic interruption | Caused by storm |
| 21 October 1993 | - | ≈10 $m^3$ | Traffic interruption | Caused by storm |
| 3 October 1994 | 04:47 | Block > 15 $m^3$ | Traffic interruption | Locomotive and first wagon slipped off the tracks |
| November 1998 | - | Six blocks ≈ 0.7 $m^3$ each | Traffic closed | Blocks stopped over the railway in the forest |
| 10 February 1999 | 17:45 | >500 $m^3$ | Facilities damage | Caused by storm |
| 2 November 1999 | 05:35 | Block ≈ 2 $m^3$ | Traffic interruption | The train stopped before the rock block |
| 27 November 1999 | - | Block ≈ 0.8 $m^3$ | Traffic closed | - |
| 16 December 2013 | - | ≈20 $m^3$ | Facilities damage | Traffic stopped for several months |

Rockfalls at the Raspadalica Cliff location were not documented until 1963, but it was noted that several occurrences reached the tracks and caused traffic interruptions. These events prompted the Railway Technical Office to construct a 120m long and 2 m high stone masonry wall at the foot of the cliff in 1964, forming a ditch to retain detached rock masses. This wall played an important role in retaining most of the small, detached blocks, but the larger blocks and fragmented material still bounced of the wall and reached the railway facilities. The rockfall mass in February 1999 hit and completely destroyed the stone wall in its central section. This section was renewed in 2000 and 2001 with 5 m high embankment [14] of coarse stone debris material.

The last major rockfall occurred on 16 December 2013 (Figure 5), which caused an interruption to railway traffic lasting several months. Following this, the construction of rockfall protection measures was conducted based on field investigations [12] and rockfall

protection design [15] and was completed in 2012. The field investigations are based on traditional in situ surveys carried out by traditional engineering geological mapping of the cliff face's rock mass, limited to a narrow accessible zone at the foot of the cliff. The design of rockfall protection [15] using rockfall protection barriers was carried out based on assumptions about the rock blocks' distribution in the cliff as well as the estimation of unstable rock block positions at the cliff, rock block volumes, and possible rockfall trajectories. The applied protection measures and rockfall barrier installation were carried out in 2014. Details of the Raspadalica Cliff analyses carried out in recent years based on new remote sensing techniques are presented in this article.

**Figure 5.** Photo of the rockfall originating from the Raspadalica Cliff on 16 December 2013.

## 3. Materials and Methods

### *3.1. Raspadalica Cliff 3D Model Establishment*

In recent years, unmanned aircraft vehicle (UAV) photogrammetry has been developed to collect spatial data. This very popular subject has found wider application in geomatics [16–21], engineering geology [21–26], and geotechnical engineering [27–33]. The products generated from UAV photogrammetry are usually datasets, such as point clouds, high-resolution digital surface models, high resolution digital orthophotos, and photo-realistic 3D models and visualizations [16,17]. Used in interdisciplinary studies, these datasets resemble high-resolution spatial data acquired by micro technology, IT systems and *structure from motion* (SfM) techniques for photogrammetric data processing. In this study a custom-made vertical takeoff and landing (VTOL) rotary wing hexacopter UAV was used as an aerial vehicle platform. The system consisted of a carbon fiber tubular frame with a radial setup of engines powered with a high-capacity lithium polymer (LiPo) battery. The total weight of the system was approximately 3.6 kg. The flight time of the system in normal conditions was about 26 min. The platform was equipped with the Pixhawk flight controller (Version: 1.8.2.) with a single-frequency GNSS receiver and additional sensors, such as gyroscopes, accelerometers, a 3-axis magnetometer, and a barometer used for navigation support. The UAV was monitored and controlled by a ground station using dual commands over the RF link. An essential component for the aerial survey was the open-source software Mission Planner (version: 1.3.50.0, firmware: APM: Copter 3.4.4), which was used for planning purposes, control, and the real-time management of the UAV.

The UAV was equipped with a Sony Alpha 7R digital camera with the 36.3-megapixel full-frame CMOS sensor (35.9 mm × 24 mm) and a high-quality Sony FE 35 mm Carl Zeiss lens.

The system used in this research has the ability to determine the 3D motion trajectory of the platform with PPK. The development of micro-technology and autonomous systems as well as the increasing demand for precise spatial data enabled the determination of the 3D trajectory using the on-board GNSS receiver and the PPK method. The raw data were stored on a memory integrated in the receiver of the moving platform. The data from the base station were able to be simultaneously stored in raw-data format or subsequently downloaded from a network service. Then, it was possible to post-process the data together with the rover data to obtain the 3D trajectory of flight and coordinates of events. In our example, the position was derived from a dual frequency Septentrio AsteRx-m UAV GNSS receiver. The reason for using the multi-rotor VTOL was its ability to assign precise positions of images captured from different positions, its applicability for many specific tasks, its ability to take-off and land with a minimal required area, and flight stability and operation at lower altitudes. In addition, the above-mentioned custom-made multirotor UAV with onboard precise positioning GNSS was able to capture full-frame high resolution oblique images of steep cliffs in the Raspadalica Cliff area.

The field survey with UAV was conducted during two flight missions. The first flight mission covered wider research area while the second flight mission was focused on a detailed survey of the cliff. During the field surveys, an area of 20 ha was covered with 273 oblique images with 80% longitudinal and lateral image overlapping. Post-processing of the 3D trajectory was performed with an image position accuracy of 3 cm planar and 5 cm in the vertical direction. The initial data processing in the office consisted of assigning the coordinates of the image center and setting up coordinate systems. The first step in the *SfM* workflow consisted of automatic identification and feature matching in multiple overlapping images using the object recognition system scale invariant feature transform (SIFT). Then, the matched feature points, along with the exact or approximate image position and orientation, were used for a bundle block adjustment procedure. The adjustment was based on 654,328 tie points. The average camera location error was 0.04 in planar and 0.05 m in vertical direction. The mean reprojection error was 0.128 pixels. Based on the 3D object reconstruction, a dense 3D high resolution point cloud (3D HRPC) with about 32 million points was generated as well as a high resolution digital surface model and orthophoto (Figure 6) with an average ground sampling distance (GSD) of 2 cm.

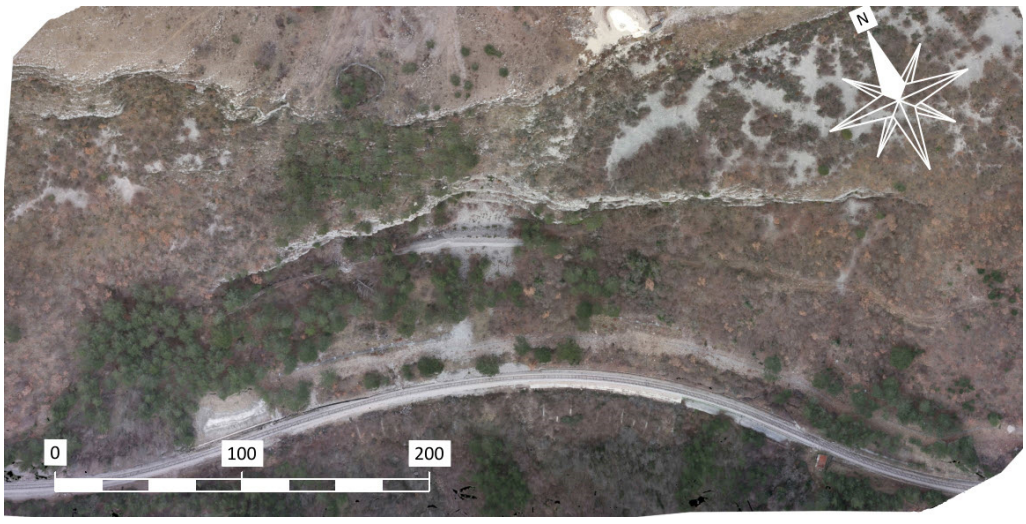


**Figure 6.** Orthophoto of Raspadalica Cliff derived from the *SfM* photogrammetry.

### 3.2. In Situ and Remote Sensing Surveys

The traditional geological and geotechnical field survey was carried out to understand the main lithology, geological formations, discontinuity sets, faults, and geotechnical geological model of the Raspadalica Cliff. The geological and geotechnical surveys were carried out at a scale of 1:500 developed for the wider zone of the cliff area. The field investigations were combined with the study at the orthophoto (at 1:5000 scale) and 3D HRPC to better understand the geological and geomorphological features at the study area. Of particular importance was the delineation of the contact between the limestone cliff structure and the flysch rock mass in the foot. A traditional geotechnical survey was conducted to determine the characteristics of the main discontinuity sets at the cliff, as well as to carry out a rock mass classification using geomechanical classification (rock mass rating, RMR) [34] and the geological strength index (GSI) [35]. Although the values of both classifications cannot play an important role in determining the rockfall process, the classifications' parameters would give a good insight into the geotechnical cliff model. As highlighted earlier, the geological and geotechnical field survey was limited to a narrow accessible zone of the rock cliff at the foot of the cliff. Field measurements of the discontinuity features and rock mass classifications were carried out at 34 accessible points at the foot of the cliff. The precision of the measurements taken was achieved within certain limits defined by the ISRM's Suggested methods for the quantitative description of discontinuities in rock masses [36].

After the establishment of the 3D HRPC model described previously, the model was analyzed to identify the main characteristics of the rock mass structure, such as the detection and mapping of the discontinuities and discontinuity sets, orientation and dip of discontinuities, spacing of discontinuities, persistence of discontinuities, and roughness of discontinues, as well as determination of rock block volumes. Due to the increasing use of UAV photogrammetry and the *SfM* technique to create 3D HRPC models, various automatic and semi-automatic techniques and methods have been developed to detect and map the discontinuities and discontinuity sets [20,22–26,28,31,37–59], orientation and dip direction of discontinuities [18,20,22,23,26,28,29,31,37–40,42–45,48,49,54–57,59–75], spacing of discontinuities [20–23,32,37,42,46,49,53,63,65,70,72,75–83], persistence of discontinuities [21,22,31,44,47,48,62,73,76,77,80,83–85], and roughness of discontinuities [22,26,37,71,86,87]. In this study, a combination of traditional geological and geotechnical field surveys [86,88] and remote sensing techniques were employed to detect and mapping of the discontinuities and discontinuity sets, orientation and dip of discontinuities, and other discontinuity features necessary for the analyses of rockfall occurrences and their consequences. Based on the identified discontinuities and discontinuity sets and their orientations and spacing, the representative block volumes were determined using the mean discontinuity spacing values for each of the discontinuity sets according to Equation (1) proposed by Palmstrom [83]:

$$V_b = S_1 \times S_2 \times S_3 \times (\sin\gamma_1 \times \sin\gamma_2 \times \sin\gamma_3), \quad (1)$$

where $S_i$ is the normal spacing and $\gamma_1$ is the angle between the discontinuity sets. While the shape of the blocks is mainly perpendicular, Equation (1) gives good data on the volumes of the blocks present in the cliff.

Based on traditional geological and geotechnical field surveys as well as the previously listed remote sensing techniques employed to identify and determine the discontinuities and discontinuity sets and their characteristic from the 3D HRPC, the structural and geotechnical model of the Raspadalica Cliff was established as the basis for identifying rockfall causes and possibilities of further rockfall occurrences.

Due to the very high uplift of the Raspadalica Cliff face and the impossibility of reaching the entire cliff face with traditional in situ geological and geotechnical surveys, a remote sensing survey based on previously described techniques was applied to the 3D HRPC model of the Raspadalica Cliff.

### 3.3. Kinematic Analysis

Once the geotechnical model of the Raspadalica Cliff was established based on the traditional geological and geotechnical field surveys and remote sensing analysis, it was possible to analyze the causes of instability and the detachment of rock blocks from the cliff face and the initiation of rockfall occurrences. Although, at first sight, the geotechnical elements of the Raspadalica Cliff do not give any clues to the causes of the frequent rockfall initiation reported in studied area, deeper analyses point to appropriate causes of instability.

The geotechnical model of the Raspadalica Cliff suggests a very low probability of the occurrence of a general circular failure through the rock mass, while the historical evidence indicates rockfalls were caused by the detachment of a specific block or group of blocks. To identify the possible causes of failure associated with the existing joint sets and their orientations, the kinematic analyses of plane, wedge, and toppling failure mechanisms [89] were performed based on the data of the joint set discontinuity features collected through both traditional geological and geotechnical field surveys and the remote sensing survey and data analysis. Kinematic analyses were performed for each cliff zone employing the Rocscience *Dips* software [90,91]. For each cliff zone, the exported discontinuity plane (facets) and orientation (dip and dip directions) data extracted using the *Cloud Compare Facet* plugin were imported into the *Dips* software, and kinematic analyses were performed for each type of failure mechanism.

## 4. Results

### 4.1. Results of the Geological and Geotechnical Survey

After the completion of the traditional geological and geotechnical field surveys and remote sensing analysis, the geotechnical model of the Raspadalica Cliff was established. Although a view of the cliff face (Figure 1) may look homogeneous from the geotechnical point of view of over the entire cliff, detailed analysis indicates five slightly different models; however, based on their properties and rock block standings, according to the general orientation and dip of cliff face zones, they should be considered and analyzed separately. These zones (Zones Z1 to Z5) are presented in the 3D HRPC (Figure 7), where the borders that separate the zones were determined by analyzing changes in the orientation and dips of the main joint sets and changes in rock block volumes.

The folding in the rock mass structure is identified during the field investigation and two folds within the cliff were identified: one fold is visible along the face of the cliff, while the other is locally visible at the location of drop blocks in the west part of the cliff (Figure 8). The folds in the eastern part (in Zones Z3 and Z4) are monocline type of fold and beds lying at two different levels and quasi-horizontal (Figure 8a, left down). In the western part of the cliff, in area of zone Z2, the remains of the anticline fold are visible; a limb of lower beds are exposed while the upper rock material collapsed in historical toppling processes (Figure 8b). This anticline fold was formed by bending due to the deformations of the lower, relatively weaker Lower Eocene flysch deposits.

The recognition of five different zones was determined based on similar discontinuity sets in each zone and carried out kinematic analyses represent possible failure mechanisms for the slopes.

The *Cloud Compare* software [92] was employed to identify discontinuity sets and their dips and dip orientations. The cliff face was divided into five zones (Figure 7), and for each segmented zone extraction of joint planes and bedding using the *Cloud Compare Facet* plugin [45,63] (Fast Marching procedure) was completed to identify their orientations (dip directions and dips). An equal area projection was used in the presentations of the joint data. Since most of the discontinuity planes belong to the joint set that is quasi-parallel to the cliff face (Joint Set 1), and the other two are nearly perpendicular and rarely exposed the joint sets (Joint Set 2 and bedding) could not be clearly recognized using the *Facet* plugin, the *Cloud Compare Compass* plugin [92] was employed to measure the joint surface orientations of the main joint sets (Figure 9).

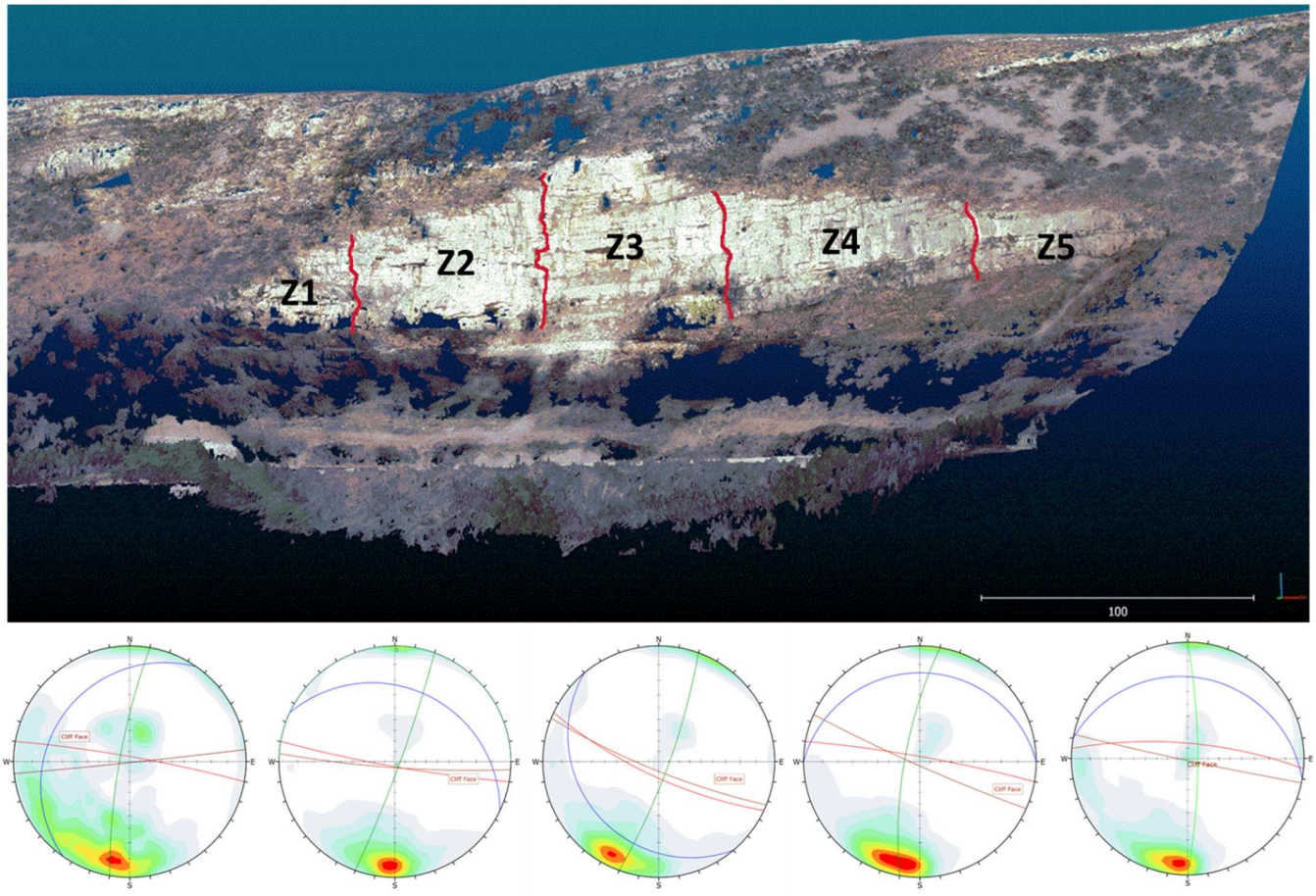


**Figure 7.** The 3D HR Point Cloud of the Raspadalica Cliff divided into five zones. For each zone the stereograph presentation of the main discontinuity sets (mean value) and orientation of the average cliff slope is presented. The concentration of plane poles quasi-parallel to cliff face is visible on each stereogram (from white (cold) with no or several poles to (hot) with high concentration of poles). Red is transversal of the average cliff face, other represent transversals of joint sets.

(**a**) (**b**)

**Figure 8.** Folds identified at the Raspadalica Cliff face: (**a**) monocline type of fold (middle part) and horizontal inclined fold (left down) in in the eastern part (in Zones Z3 and Z4); (**b**) the remains of the anticline fold western part of the cliff, in area of zone Z2 in the lower part of the figure.

The spacing between the joints for each joint set necessary to determine block volumes was determined using the *Cloud Compare Distances* tool, with which the distances in different cliff face zones were measured and analyzed. Although some developed remote sensing methods that have been successfully applied to identify other discontinuity features (separation, infilling, discontinuity wall roughness, and weathering grade) [83,86,93–97] were used in the remote sensing survey of the Raspadalica Cliff, it was found that the resulting data had too much scatter and were not as reliable as the data obtained by in situ traditional geological and geotechnical surveys.

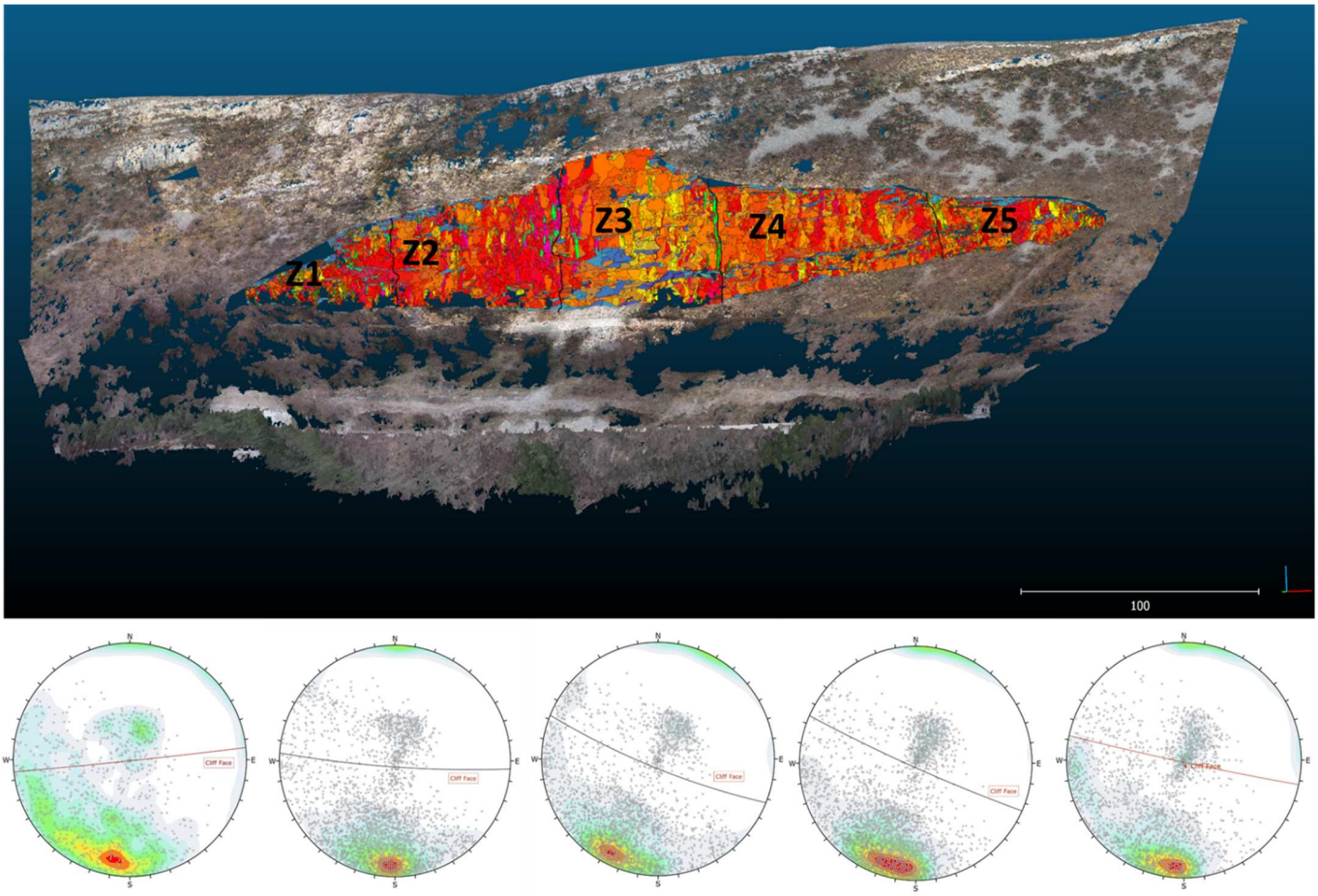


**Figure 9.** Three-dimensional HR Point Cloud of the Raspadalica Cliff with extracted facets using the *Cloud Compare Facet* plugin [43,61] (Fast Marching procedure). Orange and red to cyan facets represent Joint Set 1, parallel with the cliff face; green to yellow facets represent Joint Set 2, almost orthogonal to Joint Set 1; and blue facets represent Joint Set 3 (bedding).

Based on the statistical analyses of the data obtained from the 3D HRPC model of Raspadalica Cliff using the *Cloud Compare* software, the mean values of the orientations, discontinuity sets spacing and persistence for the total area of the Raspadalica Cliff are presented in Table 2.

**Table 2.** Values of orientations, discontinuity set spacing, and persistence obtained by remote sensing survey and analysis.

| Joint Set | Dip Direction/Dip | Discontinuity Spacing (cm) | Persistence (m) |
|---|---|---|---|
| Joint Set 1 | 8–209/73–84 | 250–500 | >20 |
| Joint Set 2 | 88–281/76–88 | 120–310 | >20 |
| Bedding | 224–307/1–23 | 10–150 | >20 |

Compared to the results obtained by traditional geological and geotechnical surveys, the remote sensing and data analysis results yielded only slightly different mean discontinuity dip directions and dip values for identically determined joint sets. These discrepancies are caused by a significantly higher number of statistically analyzed data obtained by the remote sensing survey of the entire cliff face, while the traditional geological and geotechnical surveys were limited to the accessible zone at the foot of the cliff and the low number of joint measurements. Moreover, the block volumes were visually estimated in the traditional geological and geotechnical survey, while the dimensions of the blocks were relatively precisely measured using the tools available in the *Cloud Compare* software [92].

Another important element in determining the relevant block volume is discontinuity persistence. The discontinuity size and persistence at the Raspadalica Cliff were derived from the measured length of the traces on the exposed cliff face using manual methods (scanline sampling and window sampling) in combination with various automatic and semi-automatic image analysis techniques applied to the 3D HRPC model. As long as the rock face is clearly exposed, manual sampling is a common method for discontinuity persistence determination [89]. Although the straight scanlines imply a direct measurement of the joint traces between the joint intersections on the rock slope face, in this research, most of the data were provided by measurements from the 3D HRPC model using the *Cloud Compare Distances* tool. Direct surveys were conducted at the easily accessible foot of the cliff, where detailed scanline surveys were completed [98]. Window sampling was also used for discontinuity persistence determination. Rectangular areas were selected for window sampling because of the perpendicular shape of the blocks, and the side lengths of the rectangles were twice as long as the sides of the largest blocks. The results of the manual methods were combined with the results of automatic and semi-automatic image analysis techniques [22,47,62,73,76,77,80,84,85] applied to the 3D HRPC model and used to determine the size of the relevant block.

In all zones, the traditional geological and geotechnical field surveys and remote sensing analysis indicated three main sets of mechanical discontinuities in the rock mass: one set representing bedding planes and two sets of joints approximately orthogonal to the bedding planes, forming almost parallelepiped rock blocks of different volumes. The following sections describe the results that follow from the traditional geological and geotechnical field survey and remote sensing analysis.

### In Situ Traditional Geological and Geotechnical Survey

Geologic and geotechnical investigations were conducted in an accessible area at the foot of the cliff to identify all the discontinuities and to describe all discontinuity features, such as orientation, spacing, persistence, roughness, discontinuity wall strength, aperture, degree of discontinuity wall weathering, seepage conditions, and the presence and hardness of discontinuity filling [12].

The observed discontinuities were grouped into three main sets (bedding, Joint Sets 1 and 2) as follows. Bedding dips from the NE (dip direction 0–25 degrees) to the SW and NW (dip direction: 230–305 degrees), but these variations are caused by a relatively gentle dip (15–30 degrees) and are strongly dependent on the measurement location. Joint Sets 1 and 2 are mostly subvertical with dips from 75 to 85 degrees and are nearly perpendicular sets of discontinuities, with the Joint Set 1 nearly parallel to the cliff face (dip direction: 10–30 or 155–210 degrees), while Joint Set 2 is nearly perpendicular to the cliff face and only occasionally exposed (dip direction: 90–120 or 275–280 degrees). Table 3 presents the mean values of orientations, discontinuity sets spacing, and persistence determined by in situ traditional geological and geotechnical surveys.

**Table 3.** Values of orientations, discontinuity set spacing, and persistence obtained by in situ traditional geological and geotechnical surveys.

| Joint Set | Dip Direction/Dip | Discontinuity Spacing (cm) | Persistence (m) |
|---|---|---|---|
| Joint Set 1 | 10–210/75–85 | 300–500 | >20 |
| Joint Set 2 | 90–280/75–85 | 100–300 | >20 |
| Bedding | 230–305/0–25 | 20–200 | >20 |

The other discontinuity features (separation, infilling, discontinuity wall roughness, and weathering grade) were collected and used in the following rock mass description as more reliable data about rock mass discontinuity information than the data obtained by the remote sensing survey.

### 4.2. Geotechnical Model of the Raspadalica Cliff

Based on the results of the traditional geological and geotechnical field surveys, as well as the remote sensing survey and data analysis, the geotechnical model of the Raspadalica Cliff was established, which presented the three main recognized joint sets, their orientations, and all other discontinuity features that are important for conducting stability analyses and identification of the causes of rockfall occurrences. For each of the identified zones, the mean values of joint set orientations and dip directions, as well as other discontinuity features were determined. According to the identified discontinuity features, the Geotechnical rock mass classification [34] was determined and the mean RMR values were calculated for each cliff zone. The mean values of joint set orientations and dip directions, discontinuity features, block volumes, and RMR values for each cliff zone are presented in Table 4.

### 4.3. Kinematic Analysis

The results of kinematic analyses are expressed as probability occurrence for any of possible failure mechanisms (planar sliding, direct toppling and flexural toppling; wedge failure was excluded because of very low probability of occurrence). An expression of the probability of failure occurrence was presented as kinematic hazard index by [99], as a number of failures meeting kinematic conditions of failure relative to total number of possible failures. In fact, it is not a hazard index (because of lack of temporal element), but it can express the rockfall probability for different failure modes. Additionally, the term rockfall probability must not be equated with the term susceptibility because it just points out the kinematic possibility of a failure, but not the probability of occurrence of this type of failure, which should include other parameters that have an impact on failure occurrence.

The Joint Set 2 and bedding are not so clearly expressed that their dips and dip orientations can be clearly determined, but the number of joints can be determined. The rock mass package is pretty regular, especially for the bedding, while the Joint Set 2 is regularly almost perpendicular to the most expressed Joint Set 1 and minor deviations in orientation have no impact on general results of kinematic analysis.

The results of the analyses pointed to almost no probability of wedge failure because of almost orthogonal orientation of two subvertical joint sets (Joint Sets 1 and 2), where Joint Set 1 is parallel to the cliff face. The remaining three analyzed failure mechanisms (plane, block, or direct toppling and flexural toppling) [89] indicated that these failure modes can occur at several locations of the cliff in all zones, but with a relatively low probability of occurrence. The results of the performed analyses are presented in Figure 10 and Table 5, for each zone and for each analyzed failure mechanism.

**Table 4.** The mean values of the joint set orientations and dip directions, discontinuity features, block volumes, and RMR values for each cliff zone based on results of in situ traditional geological and geotechnical surveys, remote sensing survey, and data analysis. Superscript * indicates data based on in situ traditional geological and geotechnical surveys, + indicates data based on remote sensing survey, while $^{x}$ indicates data obtained by data analysis. Abbreviations: JRC = Joint Roughness Coefficient; Weathering Grades: SW = Slightly Weathered, MW = Moderate Weathered.

| Cliff Zone | Joint Set | Mean Dip Direction/Dip + | Discontinuity Spacing (cm) + | Separation (mm) * | Infilling * | Roughness (JRC) * | Weathering Grade * | Block Volume ($m^3$) x | RMR x |
|---|---|---|---|---|---|---|---|---|---|
| Z1 | Joint set 1 | 10/85 | 300–500 | 5–100 | None | 8–10 | SW/MW | 1.2–10.0 | 58 |
| | Joint set 2 | 280/80 | 80–100 | <5 | None | 8–10 | SW/MW | | |
| | Bedding | 305/30 | 50–200 | 1–50 | Hard filling | 6–8 | SW/MW | | |
| Z2 | Joint set 1 | 190/85 | >100 | 1–5 | None | 8–10 | SW/MW | 0.5–15.0 | 60 |
| | Joint set 2 | 110/85 | 100–300 | 0.1–5 | None | 8–10 | SW/MW | | |
| | Bedding | 25/25 | 50–200 | <5 | Hard filling | 6–8 | SW/MW | | |
| Z3 | Joint set 1 | 205/75 | 50–300 | >5 | None | 4–6 | SW | 0.01–18.0 | 54 |
| | Joint set 2 | 110/80 | 20–300 | >5 | None | 4–6 | SW | | |
| | Bedding | 230/20 | 10–200 | 1–5 | Hard filling | 4–6 | SW/MW | | |
| Z4 | Joint set 1 | 10/85 | 50–300 | <5 | None | 6–8 | SW | 0.03–25.0 | 58 |
| | Joint set 2 | 280/75 | 50–300 | <5 | None | 6–8 | SW | | |
| | Bedding | 0/15 | 50–300 | <5 | Hard filling | 4–6 | SW/MW | | |
| Z5 | Joint set 1 | 5/75 | 50–300 | <5 | None | 6–8 | SW/MW | 0.05–18.0 | 58 |
| | Joint set 2 | 90/80 | 50–300 | <5 | None | 6–8 | SW/MW | | |
| | Bedding | 10/20 | 20–200 | 1–5 | Hard filling | 6–8 | SW/MW | | |

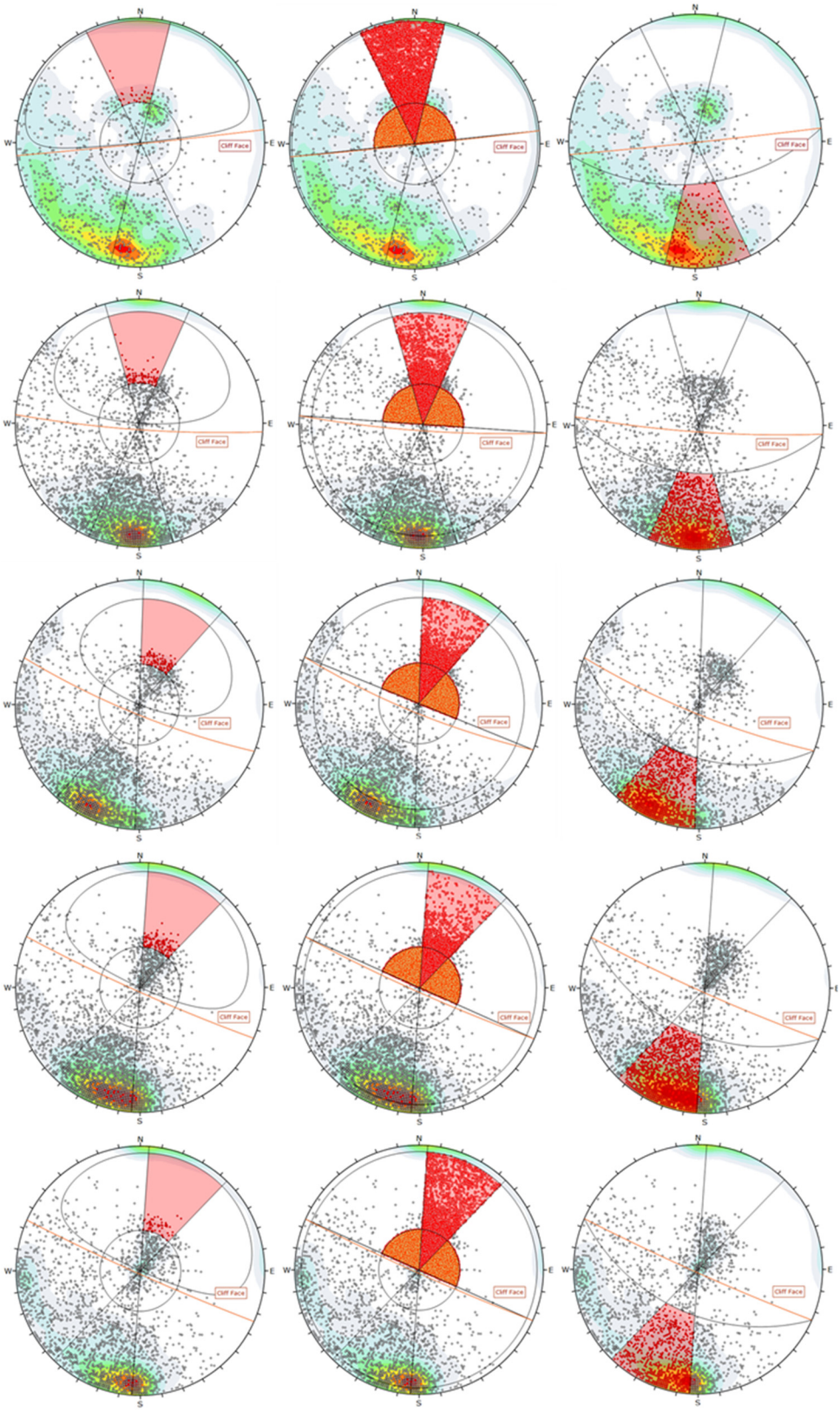


**Figure 10.** Kinematic analyses of the Raspadalica Cliff by cliff zones according to planar sliding, direct toppling and flexural toppling, conducted using Rocscience *Dips* software [91]. The results are presented in rows for each zone (e.g., Zone Z1 is in the first row). The results of planar sliding are in the first column, direct toppling in the second column, and flexural toppling in the third column.

**Table 5.** Summary of conducted kinematic analyses according to cliff zones. Probability is expressed as the ratio of number of planes (or combination of planes) meeting the conditions for a failure related to the number of all planes (or combination of planes). All planes determined in a zone are used in verification of all kinematic mechanisms.

| Cliff Zone | Type of Failure | Probability (%) | Number of Planes |
|---|---|---|---|
| Z1 | Planar sliding | 3.06 | 914 |
| | Direct toppling | 11.11 | |
| | Flexural toppling | 22.76 | |
| Z2 | Planar sliding | 3.10 | 3099 |
| | Direct toppling | 8.25 | |
| | Flexural toppling | 43.21 | |
| Z3 | Planar sliding | 3.93 | 2750 |
| | Direct toppling | 11.22 | |
| | Flexural toppling | 40.73 | |
| Z4 | Planar sliding | 3.73 | 3301 |
| | Direct toppling | 8.33 | |
| | Flexural toppling | 43.93 | |
| Z5 | Planar sliding | 2.43 | 2260 |
| | Direct toppling | 9.94 | |
| | Flexural toppling | 32.88 | |

### *4.4. Stability Analysis*

According to the results of the kinematic analyses conducted for each zone of the cliff (Zones Z1 to Z5) presented in Figure 10 and Table 5, the probability of planar sliding and direct toppling in all five zones is relatively low, while the probability of flexural toppling has a relatively high failure (>40%). Analyzing the possibility of flexural toppling at the Raspadalica Cliff, it was determined that the rock mass conditions those have significant impact on occurrence of flexural toppling are not present at the Raspadalica Cliff. The process of flexural toppling is usually formed in slopes built of continuous columns of rock separated by well-developed, steeply dipping discontinuities breaking in flexure as they bend forward. Block–flexure toppling is characterized by pseudo-continuous flexure along long columns that are divided by numerous cross joints, which are not present at Raspadalica Cliff, and there is no evidence of any block–flexural toppling failure at the Raspadalica Cliff in the past. It is very clear that in a case of flexural toppling, rockfall occurrences should be evident at the top of the cliff and not in the middle part of the rock face, as it is at the Raspadalica Cliff. Analyzing toppling stability of single blocks at the top of the cliff as well as the stability of fictive single columns to the bottom of the cliff, taking into account unfavorable dimensions and maximal determined dip of the base, neglecting the impact of friction at the side walls of a block, centers of gravity of all blocks, and fictive lie inside their bases, confirming the stability regarding toppling. Additionally, based on determined bedding and joint set dips and dip direction, no change was found in the sense of increasing the dips of the layers in the upper part of the cliff that would point to development of flexural toppling mechanisms in the cliff rock mass.

Finally, it was concluded that flexural toppling, despite the relatively high percent of possible flexural failure (>40%), is just a result of kinematic conditions for flexural toppling built into *Rocscience Dips software* [91] but has no real basis in in situ phenomena and can be neglected in further stability analyses.

The remaining two mechanisms of failure in rock mass predestined by orientations of joint sets and bedding, planar sliding, and direct toppling, have relatively very low probability of failure occurrences (planar sliding < 3.93%; direct toppling < 11.22%, Table 5) that is supported by general joint set orientations and dip directions and discontinuity features that affect stability of the cliff.

Analyzing planar sliding and direct toppling stability of the block in the Raspadalica Cliff, the geometrics and acting forces of these two mechanisms included in the analyses are schematically presented in Figure 11 (according to [90]).

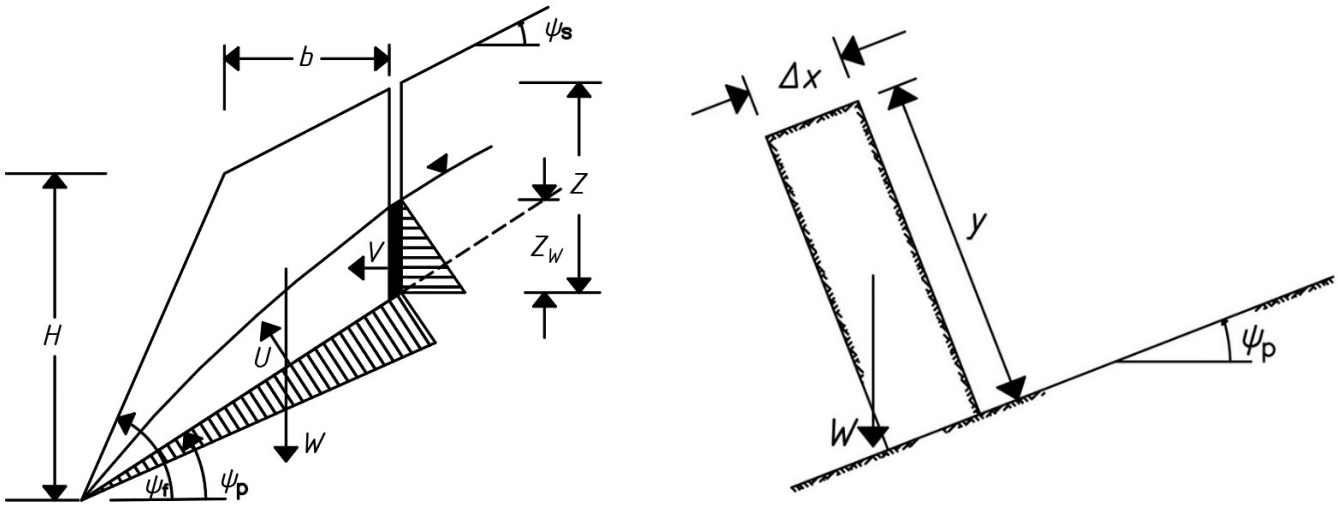


(**a**) (**b**)

**Figure 11.** Geometrics and forces of (**a**) planar sliding failure; (**b**) direct toppling failure (Reprinted with permission [90] 2004, Spoon Press).

General geometric conditions in order for planar failure to occur in the identified blocks at the Raspadalica Cliff face are satisfied [90], except that the dip of sliding plane (in this case bedding plane) must be greater than the angle of friction of this plane:

$$\Psi_p > \Phi \quad (2)$$

where $\Psi_p$ is dip of sliding plane and $\Phi$ is the angle of friction of bedding plane. According to the remote sensing survey and analyses (Table 2) and traditional geological and geotechnical surveys (Table 3), the maximal dips of the bedding plane in all cliff zones are lower than 25 degrees. If a conservative value of basic angle of friction, $\Phi_b$, is 30 degrees for limestone, that is mostly significantly lower than a real angle of friction at bedding planes, $\Phi$, which was adopted as the relevant value; therefore, it is clear that the sliding failure along the bedding plane cannot occur.

Additionally, there are several other parameters, except of basic angle of friction, that influence the strength of discontinuities: undulation or roughness expressed with the joint roughness coefficient, JRC, and joint wall compressive strength, JCS [100]. There are several other parameters that are usually not directly included in determination of the strength of discontinuities, such as separation, infilling, weathering grade of joint walls, and persistence. These parameters have an impact on the joint roughness coefficient and joint wall compressive strength. Smaller separation, together with undulation and infilling, directly influenced the strength of discontinuities: smaller separation impact on rise of the strength as well as hard filling or no filling, while the weak filling (clayey material) can significantly decrease the strength. Weathering grade of joint walls is related to joint wall compressive strength, where lower degree of weathering influences higher joint wall compressive strength. Longer persistence has no direct influence on the strength of discontinuities but has an unfavorable impact on instability mechanisms for larger volumes of rock mass.

In case of the Raspadalica Cliff and the determined characteristics of rock mass summarized in Table 4, it can be concluded that the separation of bedding and joint sets is relatively large in all cliff zones and, despite the absence of infilling and presence of hard

filling, has a negative influence on the strength of discontinuities. Measured values of the joint roughness coefficient for bedding and joint sets in all cliff zones point to smooth (JRC = 4–8) to undulating (JRC = 8–10) bedding and joint sets that just slightly influence the rise of the strength of discontinuities. At present, weathering has a very low degree of significant impact on bedding and joint set walls that is mostly slightly (SW) to moderate weathered (MW), implicating higher values of joint wall compressive strength and consequently higher values of the strength of discontinuities. In general, the conditions of bedding and joint sets in the Raspadalica Cliff can be accepted as positive in terms of bedding and joint friction increasing, and it is reasonable that for considerations of general stability, higher values of basic angle of friction for limestone ($\Phi_b$, = 31–37 degrees [100]) can be used. In particular, analyses of all three considered mechanisms (planar sliding, direct toppling, and flexural toppling) are necessary to determine the strength of discontinuities, taking into account all individual influences and the particularly crucial influence of normal stresses, as well as the possible impact of ground water.

Expressed as the factor of safety, *FoS*, along an inclined bedding plane, neglecting the impact of friction at the side walls of a block,

$$FoS = \frac{\mathrm{cA} + (\mathrm{W}\cos\Psi p - U - V\sin\Psi p)\tan\Phi}{\mathrm{W}\sin\Psi p + V\cos\Psi p} \quad (3)$$

where $c$ is cohesion; $A$ the area of sliding plane; and W, $U$, and $V$ forces are presented in Figure 11a. Neglecting cohesion at the sliding plane, and in conditions with no impact from ground water (dry conditions), Equation (3) can be written as

$$FoS = \tan\Phi/\tan\Psi_p \quad (4)$$

where, generally, all blocks in the cliff are higher than $FoS > 1.34$.

According to the previous calculation, it is very clear that planar sliding cannot occur in dry conditions. In conditions of high rainfall intensity events, a sudden rise of ground water in vertical joints behind the cliff face can be caused, and, consequently, the rise of horizontal force $V$ caused by hydrostatic water pressure and buoyancy force $U$ at the sliding plane. The rise of these forces is not high enough to cause a significant fall of the factor of safety in the upper parts of the cliff but can reduce its initial value. In the deeper parts of the cliff, the hydrostatic pressure is significantly higher, causing the extrusion of individual blocks and widening vertical joints parallel to the cliff face.

Considering the toppling failures at the Raspadalica Cliff, it was identified that most of occurred toppling failures can be determined as a secondary toppling mode [90,98], where the toppling of blocks in strong upper rock mass is due to the weathering of underlying week coal material. The weathering of coal material enabled the separation of individual blocks from upper rock mass while the bed layers formed a roof over a separated block.

In these conditions, it is possible to identify the stability of a single block (neglecting the impact of friction at the side walls of a block), as is illustrated in Figure 11b. The Figure 11b shows the conditions that indicate on stable, sliding, or toppling blocks with height of $y$ and width of $\Delta x$ on a plane dipping at an angle $\Psi_p$. Toppling occurs if when the center of gravity of the block lies outside of the base:

$$\Delta x/y < \tan\Psi_p \quad (5)$$

In the case of the Raspadalica Cliff, where the ratio between $\Delta x$ and $y$ is approximately equal to 1.0, the majority of blocks are far from the possibility of toppling. Additionally, in cases when the toppling conditions could occur, a roof over a block can prevent overturning.

As it was shown in the case of planar sliding, the stability conditions change in cases of high rainfall intensity events, as they cause a sudden rise of ground water in vertical joints behind the cliff face and, consequently, the rise of horizontal force on the blocks due to by hydrostatic water pressure. Additional horizontal hydrostatic pressure impacts the

center of gravity, moving it to the outside border of the block, but a roof over the block can prevent overturning. The result of this would be the sliding of the block along the bedding plane to the face of the cliff and moving the point of overturning inside the base of a block. Similarly to sliding mechanisms, the rise of these forces are not so efficient in the upper parts of the cliff. In the deeper parts of the cliff, the hydrostatic pressure is significantly higher, causing the extrusion of individual blocks and widening vertical joints parallel to the cliff face.

## 5. Discussion

Analysis of the results of the kinematic analysis suggests that the probability of failure occurrence (expressed as the number of failures meeting kinematic conditions of failure relative to the total number of possible failures) is relatively low and not indicative of a likely frequent occurrence of instability initiation. The results of the kinematic analyses pointed to a relatively high probability of flexural toppling, but these values should be critically considered at the Raspadalica Cliff. The process of flexural toppling is usually formed in slopes built of continuous columns of rock separated by well-developed, steeply dipping discontinuities breaking in flexure as they bend forward. Block–flexure toppling is characterized by pseudo-continuous flexure along long columns that are divided by numerous cross joints. At the Raspadalica Cliff no flexure was identified and despite the relatively high percent of possible flexural failure (>40%), the low susceptibility is determined. It is very clear that in case of flexural toppling, rockfall occurrences should be evident at the top of the cliff and not in the middle part of the rock face, as it is at the Raspadalica Cliff. To determine the objective causes of instability initiation, more detailed analyses were performed on micro locations of the cliff face from where the rock blocks were detached, leaving clear signs and geotechnical elements that caused instability. From the analysis of several main instability signs, it was found that they were caused by a combination of the joint influence of two instability mechanisms (sliding and toppling) on the rock blocks of the cliff face, as well as a rise of horizontal forces caused by groundwater rising in the vertical joints parallel to the cliff face, Figures 12 and 13.

Figure 12 presents part of Zone 3 in the middle part of the cliff. Instability 1 in the upper part of the cliff face was caused by the joint influence of sliding and toppling mechanisms and both movements (displacement and rotation) were parallel to the cliff face. The stability analyses showed that the factor of safety (FoS) for each particular mechanism is satisfactory, and only a combination of mechanisms caused rock block detachment. Instability 2 in the lower part of the cliff face was caused by the joint influence of sliding and toppling mechanisms, and both movements (displacement and toppling (rotation)) were almost orthogonal to the cliff face. The bedding plane is too slightly inclined to cause the sliding of the rock block, while the bed above the fallen block prevented toppling (rotation), but the simultaneous action of the two mechanisms allowed rockfall to be triggered in conditions where additional forces were caused by rainfall infiltration and rise of horizontal forces caused by hydrostatic pressure.

Figure 13 presents part of Zone 2 in the western part of the cliff. Instabilities 2 and 3 in the central part of the cliff face were caused by the joint influence of sliding and toppling mechanisms, and the direction of the instabilities was perpendicular to each other. The stability analyses showed that the factor of safety (FoS) for each particular mechanism was satisfactory, and only a combination of mechanisms caused the rock block detachments. The bedding planes are too slightly inclined to cause rock block sliding, while the bed above the fallen blocks prevented rotation, but the simultaneous action of two mechanisms allowed rockfall to be triggered in conditions where additional forces were caused by rainfall infiltration and rise of horizontal forces caused by hydrostatic pressure. It is not known whether these events occurred simultaneously or whether they were two separate processes.

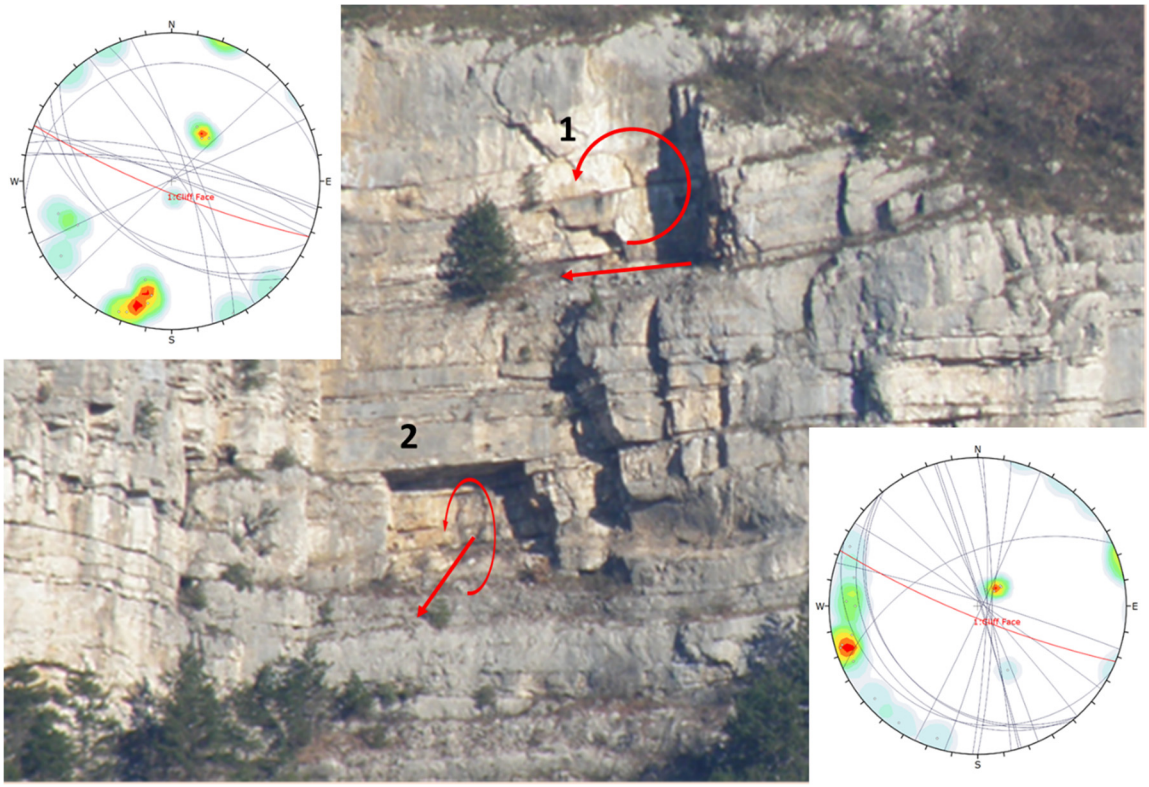


**Figure 12.** A view of the central part of the Raspadalica Cliff (Zone 3) with two signs of previous rockfall instability (1, 2). Stereographic presentations of discontinuities are present in the figure (1 left up, 2 right down) and appropriate kinematic analysis do not indicate planar or toppling instabilities.

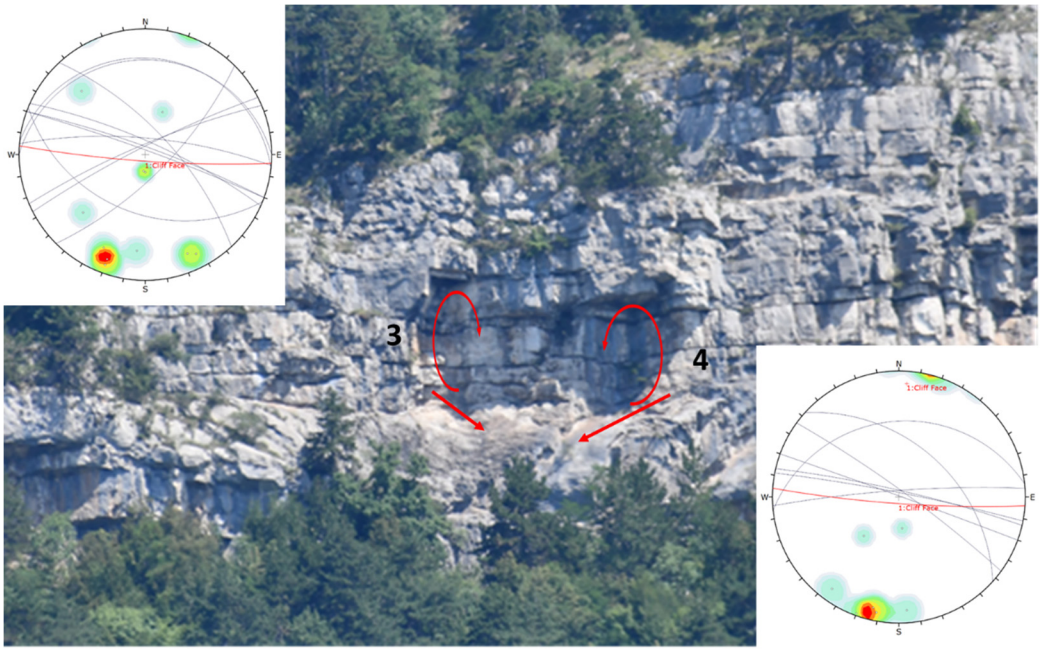


**Figure 13.** A view of the western part of the Raspadalica Cliff (Zone 2) with two signs of previous rockfall instability (3, 4). Stereographic presentations of discontinuities are present in the figure (3 left up, 4 right down,) and appropriate kinematic analyses do not indicate planar or toppling instabilities.

These two joint mechanisms are associated with some other processes related to the weakening of joint friction forces caused by lateral stress relaxation, weathering, and the

softening of joints infilling (coal interlayer) caused by freezing and thawing processes, and rock mass weathering processes, as well as by water (hydrostatic pressure of water in subvertical discontinuities, effects on the reduction of effective stresses at bedding planes) and temperature effects (pressure after freezing of water in subvertical discontinuities and the spreading and shrinkage of rock mass due to temperature effects of insolation).

There are no direct observations that accompanied registered rockfalls from the Raspadalica Cliff, but analyzing the circumstances in where the rockfalls were triggered, it is not possible to exclude any of the listed influences on the weakening of particular blocks in the cliff. Analyzing the weather conditions during the registered rockfall occurrences (listed in Table 1), it is possible to conclude that the decisive impact was caused by rainfall infiltration in vertical joints, causing a rise of hydrostatic pressure to the rock blocks in the cliff as an additional horizontal force necessary for rockfall triggering. Most of the registered rockfalls occurred during rainfall events or during storms accompanied by high rainfall intensities. It is also remarkable that the fallen rock blocks were positioned in the middle part of the cliff face, which was exposed to higher hydrostatic pressures, than the blocks in the upper parts of the cliff.

## 6. Conclusions

This manuscript presents an analysis of the rock mass structure and the causes of rockfall occurrences at the Raspadalica Cliff, Istria, Croatia; a nearly vertical, 100 m-high limestone cliff with a railway line at its foot, known for numerous rockfall occurrences in the past. In situ traditional geological and geotechnical surveys, as well as remote sensing surveys, were used to establish a geotechnical model of the cliff and to determine the causes of numerous rockfall occurrences in the past that have threatened the railway line and caused significant damage and human injuries. The aim of this manuscript is to make scientists and practitioners aware that the investigation of rock mass cliffs and possible rockfall failures must not be based on usual methods without the critical review of the obtained results and consequences. The combined use of traditional geological and geotechnical methods and more used advanced remote sensing methods leads to better modelling, while the analysis of more associated failure modes can explain the triggers of a rockfall. The traditional in situ geological and geotechnical surveys were limited to the available positions at the foot of the cliff due to the steep cliff face. Data collected by remote sensing were limited because most of the discontinuity planes belonged to the joint set that are quasi-parallel to the cliff face (Joint Set 1), while the other two nearly perpendicular and rarely exposed joint sets (Joint Set 2 and bedding) were not clearly visible and made identification of the quasi-perpendicular planes impossible. The absence of these geotechnical elements made it difficult to construct a fully defined geotechnical model of the Raspadalica Cliff and to identify the causes that initiated rockfall in the study area. Although at first glance the geotechnical elements of the Raspadalica Cliff do not provide any clues to the causes of the frequent rockfall events in the study area, deeper analyses suggest reasonable causes for rockfall instabilities. The performed kinematic stability analyses using data obtained by in situ and remote sensing surveys indicated the joint influence of two instability mechanisms (sliding and toppling) in the rock blocks of the cliff face, probably supported by additional forces, were caused by rainfall infiltration and rise of horizontal forces. These two mechanisms are associated with other processes that have influenced the weakening of joint friction forces due to lateral stress relaxation, weathering, and the softening of joints infilling (coal interlayer) caused by freezing and thawing processes, rock mass weathering processes, and water and temperature effects. These processes will continue, so rockfall occurrences at the Raspadalica Cliff can be expected in the future. The next step will be to determine rockfall hazards and risks in order to select the appropriate protection from rockfalls for the railway line in the future.

**Author Contributions:** Conceptualization, Ž.A.; methodology, Ž.A.; formal analysis, D.U. and Ž.A.; investigation, B.K., D.U. and Ž.A.; resources, D.U.; writing—original draft preparation, D.U. and Ž.A.; writing—review and editing, Ž.A.; UAV survey and visualization, B.K.; supervision, Ž.A.; project administration, Ž.A.; funding acquisition, Ž.A. All authors have read and agreed to the published version of the manuscript.

**Funding:** Part of this research was carried out in the frame of the UNIRi Project uniri-tehnic-18-276-1448 Research of Rockfall Processes and Rockfall Hazard Assessment, supported by University of Rijeka, Croatia, and the HRZZ IP-2019-04-9900 Methodology Development for Landslide Susceptibility Assessment for Land-use Planning Based on LiDAR Technology, funded by the Croatian Science Foundation. The received support is gratefully acknowledged.

**Institutional Review Board Statement:** Not applicable.

**Informed Consent Statement:** Not applicable.

**Data Availability Statement:** All data can be obtained by contacting the authors.

**Acknowledgments:** The authors would like to thank Croatian Railways Infrastructure Ltd., Technical Office Ogulin, for the data about historical rockfall occurrences at the Raspadalica Cliff location as well as Geotech Ltd., Rijeka, for the geotechnical field survey data that were used in a part of the geotechnical analysis in this study.

**Conflicts of Interest:** The authors declare no conflict of interest. The funders had no role in the design of the study; in the collection, analyses, or interpretation of data; in the writing of the manuscript, or in the decision to publish the results.

## References

1. Hungr, O.; Leroueil, S.; Picarelli, L. The Varnes Classification of Landslide Types, an Update. *Landslides* **2014**, *11*, 167–194. [CrossRef]
2. Volkwein, A.; Schellenberg, K.; Labiouse, V.; Agliardi, F.; Berger, F.; Bourrier, F.; Dorren, L.K.A.; Gerber, W.; Jaboyedoff, M. Rockfall Characterisation and Structural Protection—A Review. *Nat. Hazards Earth Syst. Sci.* **2011**, *11*, 2617–2651. [CrossRef]
3. Dorren, L.K.A. A Review of Rockfall Mechanics and Modelling Approaches. *Prog. Phys. Geogr. Earth Environ.* **2003**, *27*, 69–87. [CrossRef]
4. Emmer, A. Geographies and Scientometrics of Research on Natural Hazards. *Geosciences* **2018**, *8*, 382. [CrossRef]
5. Ritchie, A.M. Evaluation of Rockfall and Its Control. *Highw. Res. Rec.* **1963**, *17*, 13–28.
6. Siddique, T.; Pradhan, S.P.; Vishal, V. Rockfall: A Specific Case of Landslide. In *Landslides: Theory, Practice and Modelling*; Pradhan, S.P., Vishal, V., Singh, T.N., Eds.; Advances in Natural and Technological Hazards Research; Springer International Publishing: Cham, Switzerland, 2019; Volume 50, pp. 61–81. ISBN 978-3-319-77376-6.
7. Arbanas, Ž.; Benac, Č.; Jurak, V. Causes of Debris Flow Formation in Flysch Area of North Istria, Croatia. In Proceedings of the Monitoring, Simulation, Prevention and Remediation of Dense and Debris Flows, Rome, Italy, 12–14 October 2022; WIT Press: Rhodes, Greece, 2006; Volume 1, pp. 283–292.
8. Šikić, D.; Pleničar, M.; Šparica, M. *Basic Geological Map, Sheet Ilirska Bistrica, M:100.000*; Croatian Geological Survey: Zagreb, Croatia, 1975.
9. Babić, L.J.; Blašković, I.; Ferajančić, L.; Grad, K.; Grimani, I. *Basic Geological Map, Sheet Trst, M:100.000*; Geological Survey of Slovenia: Ljubljana, Slovenia, 1969.
10. Dugonjić Jovančević, S.; Arbanas, Ž. Recent Landslides on the Istrian Peninsula, Croatia. *Nat. Hazards* **2012**, *62*, 1323–1338. [CrossRef]
11. Francioni, M.; Calamita, F.; Coggan, J.; De Nardis, A.; Eyre, M.; Miccadei, E.; Piacentini, T.; Stead, D.; Sciarra, N. A Multi-Disciplinary Approach to the Study of Large Rock Avalanches Combining Remote Sensing, GIS and Field Surveys: The Case of the Scanno Landslide, Italy. *Remote Sens.* **2019**, *11*, 1570. [CrossRef]
12. Grošić, M. *Raspadalica Cliff, Geotechnical Report*; Geotech Ltd.: Rijeka, Croatia, 2012.
13. Loiotine, L.; Liso, I.S.; Parise, M.; Andriani, G.F. Optimization of Geostructural Surveys in Rock Mass Stability Analyses Using Remote Sensing Techniques. *Ital. J. Eng. Geol. Environ.* **2019**, 73–78. [CrossRef]
14. Lambert, S.; Bourrier, F. Design of Rockfall Protection Embankments: A Review. *Eng. Geol.* **2013**, *154*, 77–88. [CrossRef]
15. Grošić, M. *Raspadalica Cliff, Rockfall Protection Design*; Geotech Ltd.: Rijeka, Croatia, 2012.
16. Bishop, M.P. Remote Sensing and GIScience in Geomorphology: Introduction and Overview. In *Treatise on Geomorphology*; Elsevier: Amsterdam, The Netherlands, 2013; pp. 1–24. ISBN 978-0-08-088522-3.
17. James, M.R.; Robson, S. Straightforward Reconstruction of 3D Surfaces and Topography with a Camera: Accuracy and Geoscience Application. *J. Geophys. Res.* **2012**, *117*, F03017. [CrossRef]
18. Tannant, D. Review of Photogrammetry-Based Techniques for Characterization and Hazard Assessment of Rock Faces. *IJGE Int. J. Georesour. Environ.* **2015**, *1*, 76–87. [CrossRef]

19. Núñez-Andrés, M.A.; Buill, F.; Puig, C.; Lantada, N.; Prades, A.; Gili, J.A. Comparison of Geomatic Techniques for Rockfall Monitoring. In Proceedings of the 4th Joint International Symposium on Deformation Monitoring (JISDM), Athens, Greece, 15–17 May 2019; p. 8.
20. Nesbit, P.R.; Durkin, P.R.; Hugenholtz, C.H.; Hubbard, S.M.; Kucharczyk, M. 3-D Stratigraphic Mapping Using a Digital Outcrop Model Derived from UAV Images and Structure-from-Motion Photogrammetry. *Geosphere* **2018**, *14*, 2469–2486. [CrossRef]
21. Giordan, D.; Hayakawa, Y.; Nex, F.; Remondino, F.; Tarolli, P. Review Article: The Use of Remotely Piloted Aircraft Systems (RPASs) for Natural Hazards Monitoring and Management. *Nat. Hazards Earth Syst. Sci.* **2018**, *18*, 1079–1096. [CrossRef]
22. Giordan, D.; Adams, M.S.; Aicardi, I.; Alicandro, M.; Allasia, P.; Baldo, M.; De Berardinis, P.; Dominici, D.; Godone, D.; Hobbs, P.; et al. The Use of Unmanned Aerial Vehicles (UAVs) for Engineering Geology Applications. *Bull. Eng. Geol. Environ.* **2020**, *79*, 3437–3481. [CrossRef]
23. Francioni, M.; Simone, M.; Stead, D.; Sciarra, N.; Mataloni, G.; Calamita, F. A New Fast and Low-Cost Photogrammetry Method for the Engineering Characterization of Rock Slopes. *Remote Sens.* **2019**, *11*, 1267. [CrossRef]
24. Alptekin, A.; Çelik, M.Ö.; Doğan, Y.; Yakar, M. Mapping of a Rockfall Site with an Unmanned Aerial Vehicle. *Mersin Photogramm. J.* **2019**, *1*, 12–16.
25. Stead, D.; Donati, D.; Wolter, A.; Sturzenegger, M. Application of Remote Sensing to the Investigation of Rock Slopes: Experience Gained and Lessons Learned. *ISPRS Int. J. Geo-Inf.* **2019**, *8*, 296. [CrossRef]
26. Menegoni, N.; Giordan, D.; Perotti, C.; Tannant, D.D. Detection and Geometric Characterization of Rock Mass Discontinuities Using a 3D High-Resolution Digital Outcrop Model Generated from RPAS Imagery—Ormea Rock Slope, Italy. *Eng. Geol.* **2019**, *252*, 145–163. [CrossRef]
27. Sarro, R.; Riquelme, A.; García-Davalillo, J.; Mateos, R.; Tomás, R.; Pastor, J.; Cano, M.; Herrera, G. Rockfall Simulation Based on UAV Photogrammetry Data Obtained during an Emergency Declaration: Application at a Cultural Heritage Site. *Remote Sens.* **2018**, *10*, 1923. [CrossRef]
28. Francioni, M.; Salvini, R.; Stead, D.; Coggan, J. Improvements in the Integration of Remote Sensing and Rock Slope Modelling. *Nat. Hazards* **2018**, *90*, 975–1004. [CrossRef]
29. Vanneschi, C.; Di Camillo, M.; Aiello, E.; Bonciani, F.; Salvini, R. SfM-MVS Photogrammetry for Rockfall Analysis and Hazard Assessment Along the Ancient Roman Via Flaminia Road at the Furlo Gorge (Italy). *ISPRS Int. J. Geo-Inf.* **2019**, *8*, 325. [CrossRef]
30. Wang, S.; Zhang, Z.; Wang, C.; Zhu, C.; Ren, Y. Multistep Rocky Slope Stability Analysis Based on Unmanned Aerial Vehicle Photogrammetry. *Environ. Earth Sci.* **2019**, *78*, 260. [CrossRef]
31. Wang, S.; Ahmed, Z.; Hashmi, M.Z.; Pengyu, W. Cliff Face Rock Slope Stability Analysis Based on Unmanned Arial Vehicle (UAV) Photogrammetry. *Geomech. Geophys. Geo-Energ. Geo-Resour.* **2019**, *5*, 333–344. [CrossRef]
32. Salvini, R.; Mastrorocco, G.; Esposito, G.; Di Bartolo, S.; Coggan, J.; Vanneschi, C. Use of a Remotely Piloted Aircraft System for Hazard Assessment in a Rocky Mining Area (Lucca, Italy). *Nat. Hazards Earth Syst. Sci.* **2018**, *18*, 287–302. [CrossRef]
33. Francioni, M.; Antonaci, F.; Sciarra, N.; Robiati, C.; Coggan, J.; Stead, D.; Calamita, F. Application of Unmanned Aerial Vehicle Data and Discrete Fracture Network Models for Improved Rockfall Simulations. *Remote Sens.* **2020**, *12*, 2053. [CrossRef]
34. Bieniawski, Z.T. *Engineering Rock Mass Classifications A Complete Manual for Engineers and Geologists in Mining, Civil, and Petroleum Engineering*; Wiley-Interscience: New York, NY, USA, 1989.
35. Marinos, P.; Hoek, E. GSI: A Geologically Friendly Tool For Rock Mass Strength Estimation. In Proceedings of the ISRM International Symposium, Melbourne, Australia, 19–24 November 2000; p. 19.
36. Ulusay, R.; Hudson, J. (Eds.) *The ISRM Suggested Methods for Rock Characterization, Testing and Monitoring: 2007–2014*; Springer International Publishing: Cham, Switzerland, 2015; ISBN 978-3-319-07712-3.
37. Caudal, P.; Simonetto, E.; Merrien-Soukatchoff, V.; Dewez, T.J.B. Semi-Automatic Rock Mass Geometry Analysis from a Dense 3D Point Cloud with Discontinuitylab. *ISPRS Ann. Photogramm. Remote Sens. Spatial Inf. Sci.* **2020**, *V-2–2020*, 679–686. [CrossRef]
38. Riquelme, A.; Cano, M.; Tomás, R.; Abellán, A. Identification of Rock Slope Discontinuity Sets from Laser Scanner and Photogrammetric Point Clouds: A Comparative Analysis. *Proc. Eng.* **2017**, *191*, 838–845. [CrossRef]
39. Riquelme, A.; Abellán, A.; Tomás, R.; Jaboyedoff, M. Rock Slope Discontinuity Extraction and Stability Analysis from 3D Point Clouds: Application to an Urban Rock Slope. In Proceedings of the Vertical Geology Conference 2014, Lausanne, Switzerland, 6–7 February 2014; pp. 75–78.
40. Wong, D.; Chan, K.; Millis, S. Digital Mapping of Discontinuities. In Proceedings of the 39th HKIE Geotechnical Division Annual Seminar, Hong Kong, China, 11 April 2019; p. 13.
41. Zhang, K.; Wu, W.; Zhu, H.; Zhang, L.; Li, X.; Zhang, H. A Modified Method of Discontinuity Trace Mapping Using Three-Dimensional Point Clouds of Rock Mass Surfaces. *J. Rock Mech. Geotech. Eng.* **2020**, *12*, 571–586. [CrossRef]
42. Zhang, P.; Zhao, Q.; Tannant, D.D.; Ji, T.; Zhu, H. 3D Mapping of Discontinuity Traces Using Fusion of Point Cloud and Image Data. *Bull. Eng. Geol. Environ.* **2019**, *78*, 2789–2801. [CrossRef]
43. Buyer, A.; Schubert, W. Extraction of Discontinuity Orientations in Point Clouds. In Proceedings of the Rock Mechanics and Rock Engineering: From the Past to the Future, Ürgüp, Turkey, 29–31 August 2016; CRC Press: Cappadocia, Turkey, 2016; pp. 1133–1137.
44. Ge, Y.; Tang, H.; Xia, D.; Wang, L.; Zhao, B.; Teaway, J.W.; Chen, H.; Zhou, T. Automated Measurements of Discontinuity Geometric Properties from a 3D-Point Cloud Based on a Modified Region Growing Algorithm. *Eng. Geol.* **2018**, *242*, 44–54. [CrossRef]

45. Liu, L.; Xiao, J.; Wang, Y. Major Orientation Estimation-Based Rock Surface Extraction for 3D Rock-Mass Point Clouds. *Remote Sens.* **2019**, *11*, 635. [CrossRef]
46. Nagendran, S.K.; Mohamad Ismail, M.A.; Wen, Y.T. Photogrammetry Approach on Geological Plane Extraction Using CloudCompare FACET Plugin and Scanline Survey. *Bull. Geol. Soc. Malays.* **2019**, *68*, 151–158. [CrossRef]
47. Riquelme, A.; Tomás, R.; Cano, M.; Pastor, J.L.; Abellán, A. Automatic Mapping of Discontinuity Persistence on Rock Masses Using 3D Point Clouds. *Rock Mech. Rock Eng.* **2018**, *51*, 3005–3028. [CrossRef]
48. Anders, K.; Hämmerle, M.; Miernik, G.; Drews, T.; Escalona, A.; Townsend, C.; Höfle, B. 3D Geological Outcrop Characterization: Automatic Detection of 3D Planes (Azimuth and Dip) Using LiDAR Point Clouds. *ISPRS Ann. Photogramm. Remote Sens. Spatial Inf. Sci.* **2016**, *III–5*, 105–112. [CrossRef]
49. Buyer, A. Contributions to Block Failure Analyses Using Digital Joint Network Characterization. Ph.D. Thesis, TU Graz, Graz, Austria, 2019.
50. Bar, N.; Kostadinovski, M.; Tucker, M.; Byng, G.; Rachmatullah, R.; Maldonado, A.; Pötsch, M.; Gaich, A.; McQuillan, A.; Yacoub, T. Pit Slope Failure Evaluation in near Real Time Using UAV Photogrammetry and 3D Limit Equilibrium Analysis. *Austral. Geomech. J.* **2020**, *55*, 15.
51. Bonilla-Sierra, V.; Scholtès, L.; Donzé, F.V.; Elmouttie, M.K. Rock Slope Stability Analysis Using Photogrammetric Data and DFN–DEM Modelling. *Acta Geotech.* **2015**, *10*, 497–511. [CrossRef]
52. del Río, L.; Posanski, D.; Gracia, F.J.; Pérez-Romero, A.M. Application of Structure-from-Motion Terrestrial Photogrammetry to the Assessment of Coastal Cliff Erosion Processes in SW Spain. *J. Coast. Res.* **2020**, *95*, 1057. [CrossRef]
53. Donati, D.; Stead, D.; Ghirotti, M.; Wolter, A. A Structural Investigation of the Hope Slide, British Columbia, Using Terrestrial Photogrammetry and Rock Mass Characterization. *Rend. Online Soc. Geol. Ital.* **2013**, *24*, 107–109.
54. Drews, T.; Miernik, G.; Anders, K.; Höfle, B.; Profe, J.; Emmerich, A.; Bechstädt, T. Validation of Fracture Data Recognition in Rock Masses by Automated Plane Detection in 3D Point Clouds. *Int. J. Rock Mech. Min. Sci.* **2018**, *109*, 19–31. [CrossRef]
55. Farmakis, I.; Marinos, V.; Papathanassiou, G.; Karantanellis, E. Automated 3D Jointed Rock Mass Structural Analysis and Characterization Using LiDAR Terrestrial Laser Scanner for Rockfall Susceptibility Assessment: Perissa Area Case (Santorini). *Geotech Geol. Eng.* **2020**, *38*, 3007–3024. [CrossRef]
56. Karantanellis, E.; Marinos, V.; Vassilakis, E.; Christaras, B. Object-Based Analysis Using Unmanned Aerial Vehicles (UAVs) for Site-Specific Landslide Assessment. *Remote Sens.* **2020**, *12*, 1711. [CrossRef]
57. Menegoni, N.; Giordan, D.; Perotti, C. Reliability and Uncertainties of the Analysis of an Unstable Rock Slope Performed on RPAS Digital Outcrop Models: The Case of the Gallivaggio Landslide (Western Alps, Italy). *Remote Sens.* **2020**, *12*, 1635. [CrossRef]
58. Robiati, C.; Eyre, M.; Vanneschi, C.; Francioni, M.; Venn, A.; Coggan, J. Application of Remote Sensing Data for Evaluation of Rockfall Potential within a Quarry Slope. *SPRS Int. J. Geo-Inf.* **2019**, *8*, 367. [CrossRef]
59. Nagendran, S.K.; Mohamad Ismail, M.A.; Tung, W.Y. 2D and 3D Rock Slope Stability Assessment Using Limit Equilibrium Method Incorporating Photogrammetry Technique. *BGSM* **2019**, *68*, 133–139. [CrossRef]
60. Guo, J.; Liu, Y.; Wu, L.; Liu, S.; Yang, T.; Zhu, W.; Zhang, Z. A Geometry- and Texture-Based Automatic Discontinuity Trace Extraction Method for Rock Mass Point Cloud. *Int. J. Rock Mech. Min. Sci.* **2019**, *124*, 104132. [CrossRef]
61. Guo, J.; Wu, L.; Zhang, M.; Liu, S.; Sun, X. Towards Automatic Discontinuity Trace Extraction from Rock Mass Point Cloud without Triangulation. *Int. J. Rock Mech. Min. Sci.* **2018**, *112*, 226–237. [CrossRef]
62. Kong, D.; Wu, F.; Saroglou, C. Automatic Identification and Characterization of Discontinuities in Rock Masses from 3D Point Clouds. *Eng. Geol.* **2020**, *265*, 105442. [CrossRef]
63. Zhang, Y.; Yue, P.; Zhang, G.; Guan, T.; Lv, M.; Zhong, D. Augmented Reality Mapping of Rock Mass Discontinuities and Rockfall Susceptibility Based on Unmanned Aerial Vehicle Photogrammetry. *Remote Sens.* **2019**, *11*, 1311. [CrossRef]
64. Dewez, T.J.B.; Girardeau-Montaut, D.; Allanic, C.; Rohmer, J. Facets: A CloudCompare Plugin to Extract Geological Planes from Unstructured 3D Point Clouds. *Int. Arch. Photogramm. Remote Sens. Spatial Inf. Sci.* **2016**, *XLI-B5*, 799–804. [CrossRef]
65. Riquelme, A.; Tomás, R.; Cano, M.; Abellán, A. Using Open-Source Software for Extracting Geomechanical Parameters of a Rock Mass from 3D Point Clouds: Discontinuity Set Extractor and SMRTool. In *Rock Mechanics and Rock Engineering: From the Past to the Future*; CRC Press: Cappadocia, Turkey, 2016; pp. 1091–1096.
66. Tung, W.Y.; Nagendran, S.K.; Mohamad Ismail, M.A. 3D Rock Slope Data Acquisition by Photogrammetry Approach and Extraction of Geological Planes Using FACET Plugin in CloudCompare. *IOP Conf. Ser. Earth Environ. Sci.* **2018**, *169*, 012051. [CrossRef]
67. Chesley, J.T.; Leier, A.L.; White, S.; Torres, R. Using Unmanned Aerial Vehicles and Structure-from-Motion Photogrammetry to Characterize Sedimentary Outcrops: An Example from the Morrison Formation, Utah, USA. *Sediment. Geol.* **2017**, *354*, 1–8. [CrossRef]
68. Eltner, A.; Sofia, G. Structure from motion photogrammetric technique. In *Developments in Earth Surface Processes*; Elsevier: Amsterdam, The Netherlands, 2020; Volume 23, pp. 1–24. ISBN 978-0-444-64177-9.
69. Liu, C.; Liu, X.; Peng, X.; Wang, E.; Wang, S. Application of 3D-DDA Integrated with Unmanned Aerial Vehicle–Laser Scanner (UAV-LS) Photogrammetry for Stability Analysis of a Blocky Rock Mass Slope. *Landslides* **2019**, *16*, 1645–1661. [CrossRef]
70. Mancini, F.; Castagnetti, C.; Rossi, P.; Dubbini, M.; Fazio, N.; Perrotti, M.; Lollino, P. An Integrated Procedure to Assess the Stability of Coastal Rocky Cliffs: From UAV Close-Range Photogrammetry to Geomechanical Finite Element Modeling. *Remote Sens.* **2017**, *9*, 1235. [CrossRef]

71. Mikita, T.; Balková, M.; Bajer, A.; Cibulka, M.; Patočka, Z. Comparison of Different Remote Sensing Methods for 3D Modeling of Small Rock Outcrops. *Sensors* **2020**, *20*, 1663. [CrossRef] [PubMed]
72. Nagendran, S.K.; Mohamad Ismail, M.A.; Tung, W.Y. Integration of UAV Photogrammetry and Kinematic Analysis for Rock Slope Stability Assessment. *Bull. Geol. Soc. Malays.* **2019**, *67*, 105–111. [CrossRef]
73. Riquelme, A.J.; Abellán, A.; Tomás, R.; Jaboyedoff, M. A New Approach for Semi-Automatic Rock Mass Joints Recognition from 3D Point Clouds. *Comput. Geosci.* **2014**, *68*, 38–52. [CrossRef]
74. Riquelme, A.J.; Tomás, R.; Abellán, A. Characterization of Rock Slopes through Slope Mass Rating Using 3D Point Clouds. *Int. J. Rock Mech. Min. Sci.* **2016**, *84*, 165–176. [CrossRef]
75. Zekkos, D.; Greenwood, W.; Lynch, J.; Manousakis, J.; Athanasopoulos-Zekkos, A.; Clark, M.; Saroglou, C. Lessons Learned from The Application of UAV-Enabled Structure-From-Motion Photogrammetry in Geotechnical Engineering. *Int. J. Geoeng. Case Hist.* **2018**, *4*, 254–274. [CrossRef]
76. Brugger, M.; Sellmeier, B.; Menschik, F.; Käsling, H.; Thuro, K. The Scope of Photogrammetry and TLS in the Context of Geomechanical Discontinuity Analysis. In *IAEG/AEG Annual Meeting Proceedings, San Francisco, California, 2018—Volume 1*; Shakoor, A., Cato, K., Eds.; Springer International Publishing: Cham, Switzerland, 2019; pp. 311–316. ISBN 978-3-319-93123-4.
77. Buyer, A.; Schubert, W. Joint Trace Detection in Digital Images. In Proceedings of the 10th Asian Rock Mechanics Symposium, Singapore, 29 October–3 November 2018; p. 11.
78. Buyer, A.; Schubert, W. Calculation the Spacing of Discontinuities from 3D Point Clouds. *Proc. Eng.* **2017**, *191*, 270–278. [CrossRef]
79. Riquelme, A.J.; Abellán, A.; Tomás, R. Discontinuity Spacing Analysis in Rock Masses Using 3D Point Clouds. *Eng. Geol.* **2015**, *195*, 185–195. [CrossRef]
80. Bonetto, S.; Umili, G.; Ferrero, A.M.; Carosi, R.; Simonetti, M.; Biasi, A.; Migliazza, M.R.; Bianchini, S. Geostructural and Geomechanical Study of the Piastrone Quarry (Seravezza, Italy) Supported by Photogrammetry to Assess Failure Mode. *Geosciences* **2020**, *10*, 64. [CrossRef]
81. Donati, D.; Stead, D.; Brideau, M.-A.; Ghirotti, M. Using Pre-Failure and Post-Failure Remote Sensing Data to Constrain the Three-Dimensional Numerical Model of a Large Rock Slope Failure. *Landslides* **2021**, *18*, 827–847. [CrossRef]
82. Guerin, A.; Jaboyedoff, M.; Collins, B.D.; Derron, M.-H.; Stock, G.M.; Matasci, B.; Boesiger, M.; Lefeuvre, C.; Podladchikov, Y.Y. Detection of Rock Bridges by Infrared Thermal Imaging and Modeling. *Sci. Rep.* **2019**, *9*, 13138. [CrossRef] [PubMed]
83. Palmstrom, A. *Measurement and Characterization of Rock Mass Jointing*; Sharma, V.M., Saxena, K.R., Eds.; A. A. Balkema Publishers: Lisse, The Netherlands; Abingdon, UK; Exton, PA, USA; Tokio, Japan, 2001.
84. Zhang, W.; Lan, Z.; Ma, Z.; Tan, C.; Que, J.; Wang, F.; Cao, C. Determination of Statistical Discontinuity Persistence for a Rock Mass Characterized by Non-Persistent Fractures. *Int. J. Rock Mech. Min. Sci.* **2020**, *126*, 104177. [CrossRef]
85. Zhang, W.; Wang, J.; Xu, P.; Lou, J.; Shan, B.; Wang, F.; Cao, C.; Chen, X.; Que, J. Stability Evaluation and Potential Failure Process of Rock Slopes Characterized by Non-Persistent Fractures. *Nat. Hazards Earth Syst. Sci.* **2020**, *20*, 2921–2935. [CrossRef]
86. Mastrorocco, G.; Salvini, R.; Esposito, G.; Seddaiu, M. 3D Point Cloud Analysis for Surface Roughness Measurement: Application of UAV Photogrammetry. *Rend. Online Soc. Geol. Ital.* **2016**, *41*, 313–316. [CrossRef]
87. Salvini, R.; Vanneschi, C.; Coggan, J.S.; Mastrorocco, G. Evaluation of the Use of UAV Photogrammetry for Rock Discontinuity Roughness Characterization. *Rock Mech Rock Eng.* **2020**, *53*, 3699–3720. [CrossRef]
88. Bolla, A.; Paronuzzi, P. Geomechanical Field Survey to Identify an Unstable Rock Slope: The Passo Della Morte Case History (NE Italy). *Rock Mech Rock Eng.* **2020**, *53*, 1521–1544. [CrossRef]
89. Shang, J.; West, L.J.; Hencher, S.R.; Zhao, Z. Geological Discontinuity Persistence: Implications and Quantification. *Eng. Geol.* **2018**, *241*, 41–54. [CrossRef]
90. Wyllie, D.C.; Mah, C.W. *Rock Slope Engineering: Civil and Mining*, 4th ed.; Spon Press: London, UK; New York, NY, USA, 2004; p. 456.
91. Available online: http://https://www.rocscience.com/software/dips (accessed on 10 May 2021).
92. Available online: http://www.cloudcompare.org/doc/qCC/CloudCompare%20v2.6.1%20-%20User%20manual.pdf (accessed on 12 March 2021).
93. Draebing, D.; Krautblatter, M. The Efficacy of Frost Weathering Processes in Alpine Rockwalls. *Geophys. Res. Lett.* **2019**, *46*, 6516–6524. [CrossRef]
94. Gratchev, I.; Pathiranagei, S.V.; Kim, D.H. Strength Properties of Fresh and Weathered Rocks Subjected to Wetting–Drying Cycles. *Geomech. Geophys. Geo-Energ. Geo-Resour.* **2019**, *5*, 211–221. [CrossRef]
95. Francioni, M.; Sciarra, N.; Ghirotti, M.; Borgatti, L.; Salvini, R.; Calamita, F. The Impact of New Technologies in the Engineering Classification of Rock Masses. *Ital. J. Eng. Geol. Environ.* **2019**, 33–39. [CrossRef]
96. Pagano, M.; Palma, B.; Ruocco, A.; Parise, M. Discontinuity Characterization of Rock Masses through Terrestrial Laser Scanner and Unmanned Aerial Vehicle Techniques Aimed at Slope Stability Assessment. *Appl. Sci.* **2020**, *10*, 2960. [CrossRef]
97. Popov, V.I. Frost Weathering as a Process of Degradation of Surface of Rocks under the Action of Internal Stresses. *IOP Conf. Ser. Earth Environ. Sci.* **2020**, *459*, 052018. [CrossRef]
98. Hencher, S. *Practical Rock Mechanics*; Taylor & Francis: Boca Raton, FL, USA, 2015.
99. Casagli, N.; Pini, G. Analisi cinematica della stabilità di versanti naturali e fronti di scavo in roccia. *Geol. Appl. Idrogeol.* **1993**, *28*, 223–232. (In Italian)
100. Barton, N.; Choubey, V. The shear strength of rock joints in theory and practice. *Rock Mech.* **1977**, *10*, 1–54. [CrossRef]